Global and Planetary Change 165 (2018) 62–89

Contents lists available at ScienceDirect

Global and Planetary Change

journal homepage: www.elsevier.com/locate/gloplacha

Invited research article

Decades of urban growth and development on the Asian megadeltas

Christopher Small[a,*], Daniel Sousa[a], Gregory Yetman[b], Christopher Elvidge[c], Kytt MacManus[b]

[a] Lamont Doherty Earth Observatory, Columbia University, Palisades, NY, USA
[b] CIESIN, Columbia University, Palisades, NY, USA
[c] Earth Observation Group, NCEI, NOAA, Boulder, CO, USA

ABSTRACT

The current and ongoing expansion of urban areas worldwide represents the largest mass migration in human history. It is well known that the world's coastal zones are associated with large and growing concentrations of population, urban development and economic activity. Among coastal environments, deltas have long been recognized for both benefits and hazards. This is particularly true on the Asian megadeltas, where the majority of the world's deltaic populations reside. Current trends in urban migration, combined with demographic momentum suggest that the already large populations on the Asian megadeltas will continue to grow. In this study, we combine recently released gridded population density (circa 2010) with a newly developed night light change product (1992 to 2012) and a digital elevation model to quantify the spatial distribution of population and development on the nine Asian megadeltas. Bivariate distributions of population as functions of elevation and coastal proximity quantify potential exposure of deltaic populations to flood and coastal hazards. Comparison of these distributions for the Asian megadeltas show very different patterns of habitation with peak population elevations ranging from 2 to 11 m above sea level over a wide range of coastal proximities. Over all nine megadeltas, over 174 million people reside below a peak population elevation of 7 m. Changes in the spatial extent of anthropogenic night light from 1992 to 2012 show widely varying extents and changes of lighted urban development. All of the deltas except the Indus show the greatest increases in night light brightness occurring at elevations < 10 m. At global and continental scales, growth of settlements of all sizes takes the form of evolving spatial networks of development. Spatial networks of lighted urban development in Asia show power law scaling properties consistent with other continents, but much higher rates of growth. The three largest networks of development in China all occur on deltas and adjacent lowlands, and are growing faster than the rest of the urban network in China. Since 2000, the Huanghe Delta + North China Plain urban network has surpassed the Japanese urban network in size and may soon connect with the Changjiang Delta + Yangtze River urban network to form the largest conurbation in Asia.

1. Introduction

The current and ongoing expansion of urban areas worldwide represents the largest mass migration in human history. The percentage of global population considered to be urban has risen from 30% in 1950 to 54% in 2014 and is projected to reach 66% by 2050 (United Nations, 2015). Although the population of Asia is currently only 40% urban, it already accounts for 53% of the world's urban population. By 2050, India and China are projected to have urban populations of 404 and 292 million (respectively). However, almost half of the global urban population lives in cities of < 500,000 while < 1/8 lives in megacities of > 10 million inhabitants.

It is well known that the world's coastal zones are associated with large and growing concentrations of population, urban development and economic activity. The global population living within 100 km of a shoreline at elevations < 100 m has been estimated at 1.2×10^9 people (circa 1990) with an average population density nearly three times higher than global average density (Small and Nicholls, 2003). Within this coastal zone, the highest mean population densities occur over a range of coastal proximity reflecting large populations in low-lying river basins and deltas. Consistent with the findings of the United Nations (2015)), this comparison of satellite observed night light and census-derived population indicates that most of this coastal population occurs in relatively densely populated rural areas and small to medium size cities rather than large cities.

Deltas have long been recognized for both benefits and hazards. The benefits of fertile soils and fluvial to coastal transportation corridors are balanced by a variety of coastal and flood hazards (Nicholls et al.,

* Corresponding author.
E-mail address: csmall@columbia.edu (C. Small).

https://doi.org/10.1016/j.gloplacha.2018.03.005
Received 3 November 2017; Received in revised form 14 February 2018; Accepted 12 March 2018
Available online 27 March 2018
0921-8181/

2007). Over 325 million people live on deltas worldwide (Syvitski and Saito, 2007) with > 250 million (circa 2000) on nine Asian deltas alone (Woodroffe et al., 2006). These so-called Asian megadeltas are of particular interest because they are among the most densely populated and rapidly urbanizing environments on Earth. In addition to the well known coastal and fluvial hazards posed by the deltaic environment, human activities are also known to impact the dynamics of deltas through the disruption of water flow (Vörösmarty and Sahagian, 2000) and sediment delivery (Syvitski and Saito, 2007). Interruption of sediment delivery by upstream capture (Syvitski et al., 2005) and flood control measures, compounded by natural and human-induced subsidence (Syvitski et al., 2009) results in a rise in relative sea level generally in excess of the rate of eustatic sea level rise, contributing to increased levels of inundation and coastal erosion (Ericson et al., 2006). This feedback between increasing levels of development and increasing vulnerability depends critically on the spatial extent, location and type of development within the deltaic environment. This is particularly true on the Asian megadeltas where current rate of urban development has been increasing over the past 20 years.

In this study, we combine recently released gridded population density (circa 2010) with a newly developed night light change product (1992 to 2013) and a digital elevation model to quantify the spatial distribution of population and development within the nine Asian megadeltas. While the earlier study of (Small and Nicholls, 2003) quantified the global distribution of population and development in coastal zones at continental and regional scales, the population and elevation products available at that time did not have sufficient spatial resolution or vertical accuracy (respectively) to quantify the relationship at spatial scales appropriate for most deltas. The gridded population data used in this study vary in spatial resolution from country to country, but generally provide sufficient resolution (10–50 km) to distinguish the higher densities associated with large cities and their location with respect to shorelines and sea level. We quantify the distribution of population with respect to coastal proximity and elevation to allow comparison among deltas. We use satellite-derived maps of night light brightness as a proxy for urban development coinciding with outdoor lighted infrastructure. While not all forms of development coincide with outdoor lighting, and some outdoor lighting is not related to urban development (e.g. resource extraction, fishing, fires, etc), the land areas under consideration in this study do not include significant areas of non-urban lighting. The night light change product provides much higher spatial resolution (0.5–2.5 km) and clearly resolves the location and spatial extent of urban development since 1992. We quantify this change in lighted development on the megadeltas in the context of rapid spatiotemporal evolution of networks of urban development throughout southeastern Asia over the past 25 years. We take the work of (Woodroffe et al., 2006) as a starting point for an intercomparison of the Asian megadeltas in the context of population distribution and evolution of lighted development and attempt to interpret this evolution in the context of the ongoing rapid urban growth occurring throughout Asia.

2. Data

The spatial extent of each delta is based on the spatial extent of the maximum transgression at highstand 6000 years ago as defined by Woodroffe et al. (2006). Each delta study area was chosen to completely encompass the corresponding delta as defined by Woodroffe et al. (2006). The boundaries of the delta are also apparent on the bivariate distributions as departures from the overall elevation gradient extending inland. As noted by Woodroffe et al. (2006), “SRTM analysis of those deltas for which the maximum transgression has been mapped confirms that this margin coincides with a marked change in gradient. “.

2.1. Population

Population counts and densities were obtained from the Gridded Population of the World v.4 (GPW4) available from the Socioeconomic Data and Applications Center (SEDAC) at http://sedac.ciesin.columbia.edu/data/collection/gpw-v4. The 30″ grids were coregistered with elevation and night light grids (described below) and resampled to 15″ to preserve the full resolution of the VIIRS DNB night light product.

Input data sources for GPW4 are obtained from National Statistical Offices, National Mapping Agencies, and alternative international sources when necessary. Priority is given to official national sources at the highest possible spatial resolution, but in cases where there is no official source, or that information cannot be acquired, alternative sources are used. The GPW4 metadata and documentation includes information about the citation and spatial resolution for all data sources.

GPW4 allocates population from areal administrative, or enumeration, polygons into grid cells using a uniform proportional allocation method. Input polygons are overlaid with an inland water dataset comprised of various national and international sources in order to eliminate inland water areas from the gridding process. Land areas are calculated at the national level based on a custom Mollweide Equal Area Projection centered on each country. Population is finally distributed equally on the basis of the ratio of the land area in a given pixel to the total land area of its parent census geometry.

GPW4 is based on > 13 million input census geographies at varying spatial resolution. The size of these input units varies among and within countries, and generally consists of higher resolution geographies in and around cities, and lower resolutions in areas where there are less people. Where the resolution of an input census geography is coarse, the uniform proportional allocation approach can lead to reduced precision and accuracy at the pixel scale. The GPW4 data collection includes a data quality layer on the Mean Administrative Area of input units which should be consulted when using the dataset. This data quality layer can be used as a guide for the appropriate size of a study area within a region. If the size of a study area is smaller than the size of the mean administrative area in that location, then descriptive statistics and aggregation on that area cannot be relied upon with confidence. In other words, the size of a study area should always be larger than the mean administrative unit area when using GPW4 data. The mean equivalent square length for the administrative units in each delta study area is given on the inset population density map in the a) figure for each delta.

Although GPW population estimates are available for multiple years, we use only the totals from the census year (nominally 2010) and make no attempt to estimate population change at the scale of the individual grid cell. The GPW population time series are adjusted to target years using growth rates from two census dates and interpolation or extrapolation as appropriate. The rates are calculated at aggregated census levels (state/province or district) to facilitate matching between the two census dates. The use of aggregated census data for interpolation and extrapolation masks differences in change over time at the local level; in most cases, the GPW data are only useful for calculating change at the regional level. Therefore, we only use the nominal 2010 population distribution as a measure of the overall spatial distribution of people in each study area. While we do provide aggregate population change estimates at the scale of each delta, spatially explicit change analysis is limited to spatiotemporal changes in night light between 1992 and 2012.

We prefer the proportional allocation densities from GPW4 to other population distribution products because these densities are based on only one assumption – uniform spatial distribution within each administrative unit. Even though populations are known to cluster at scales much finer than any of these administrative units, the clustering is known to be time and space dependent so any assumptions used to disaggregate census data to finer spatial scales are generally of

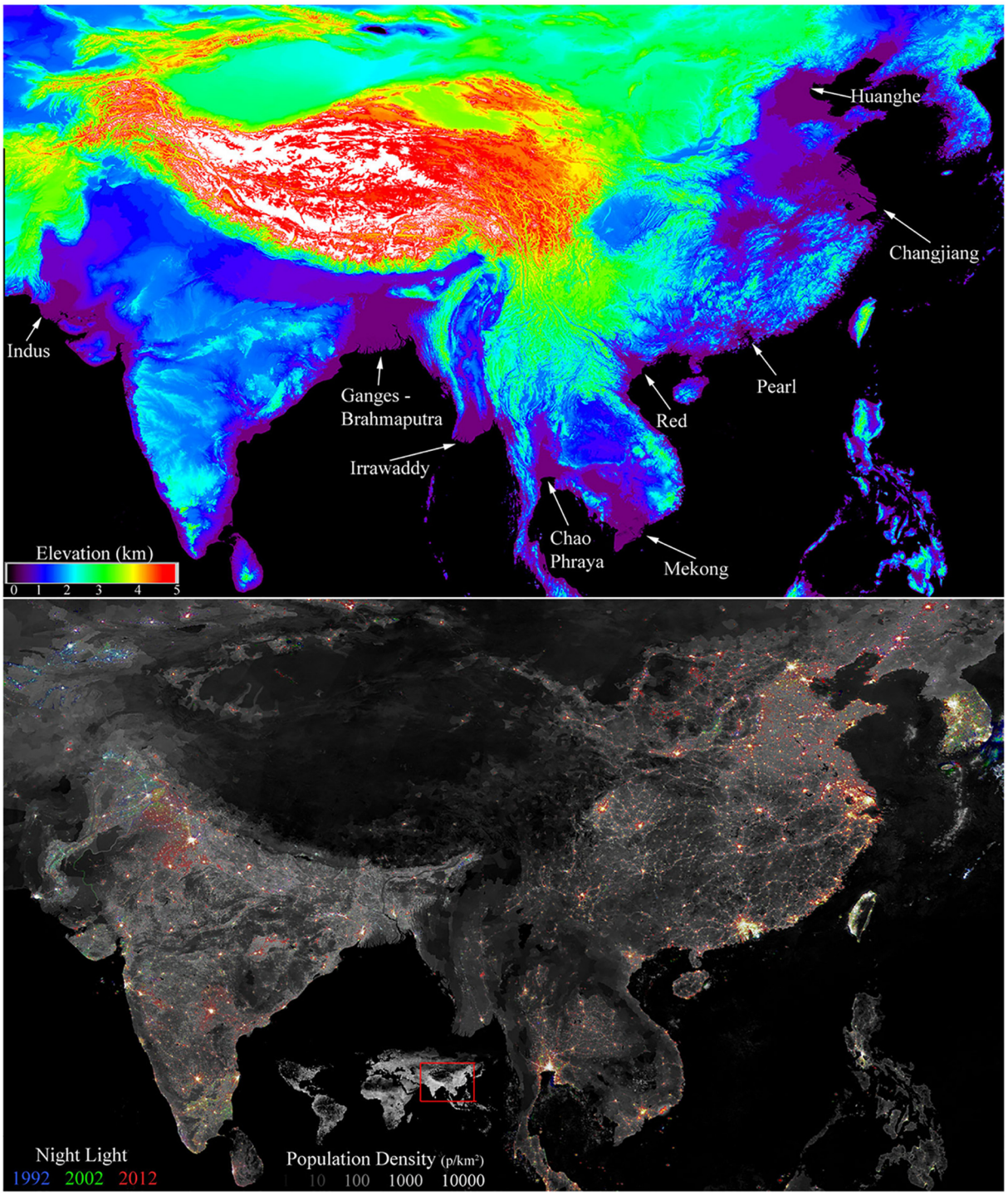

Fig. 1. People and deltas in southeastern Asia. Warmer colors on lower map show increasing development post-1992.

unknown validity. While there are a potentially infinite number of disaggregated population distributions possible at sub-kilometer scales, the uniform distribution assumption is an important endmember case because it represents the most conservative estimate of population distribution within the constraints of the administrative boundaries from which the population estimates are ultimately derived.

2.2. Night light

DMSP-OLS and VIIRS DNB night light composites were obtained from the NOAA Earth Observation Group (https://ngdc.noaa.gov/eog/). The VIIRS day/night band (DNB) collects nighttime low-light imaging data similar to the DMSP predecessor, with several major improvements (Elvidge et al., 2013). The VIIRS has in-flight calibration, a pixel footprint 45 times smaller than DMSP, lower detection limits, wider dynamic range, and quantization is increase from 6 to 14 bits. The basic procedures used to make VIIRS nighttime lights are similar to those used for the DMSP time series (Elvidge et al., 2017). Annual composites of DMSP-OLS night light from 1992 to 2013, gridded at 30″, were intercalibrated using the procedure given by Elvidge et al. (2009) but with updated intercalibration coefficients developed for the Version 4 product. Each DMSP composite was coregistered with a VIIRS DNB night light composite from June 2013

at 15″ resolution. Full annual time series of OLS brightness were used to generate the brightness trajectory plots of individual pixels shown in each delta figure. These trajectories give an indication of the types of night light change observable by OLS. To make the tri-temporal composites, only the 1992, 2002 and 2012 composites were used. The dOLS + VIIRS image fusion procedure (described below) is used to show the current (circa 2013) extent of lighted development at VIIRS' full spatial resolution in conjunction with changes in brightness and extent from OLS since 1992.

2.3. Elevation

The SRTM (v2.1) DEMs were obtained from the USGS (http://earthexplorer.usgs.gov) in the form of 1 arc *sec* (1″ = ~28 m at 40°N) resolution geographic grids in the WGS84 horizontal and EGM96 vertical reference systems. The 1″ grids were resampled using cubic convolution to provide mean elevations at the 15″ resolution of the VIIRS night light grids.

The accuracy and resolution of SRTM in coastal environments with relatively small differences in elevation over large areas are of particular relevance to this study. At low elevations and slopes the magnitude of the radar signal approaches the noise level of the measurements, reducing the absolute accuracy of the elevation estimate - which can lead to large errors in inundation estimates on low gradient environments like deltas. This is especially relevant for developed coastal environments where the spatial extent of inundation can have disproportionate consequences in terms of loss of life and property. There have been several comparative analyses of global DEM vertical accuracy (e.g. (Gesch et al., 2012, Meyer et al., 2012), (Tachikawa et al., 2011, Tadono et al., 2012), (Smith and Sandwell, 2003)). Some analyses have included coastal areas (e.g. (Gorokhovich and Voustianiouk, 2006), (Hvidegaard et al., 2012)), and some have incorporated land cover/use information (e.g. (Gesch et al., 2012), (Hofton et al., 2006), (Carabajal and Harding, 2006)), but developed coastal environments are not addressed specifically by these studies. To address coastal DEM accuracy specifically, (Small and Sohn, 2015) compared the 1" SRTM DEM (and GDEM2) with a sub-meter resolution LiDAR-derived DEM in a variety of coastal environments in NYC. Compared to the LiDAR DEM, SRTM had a positive bias of 1.9 m and an uncertainty of 3.6 m. Cross spectral analysis of the LiDAR and SRTM DEMs indicated a correlation scale of 500 m below which coherency of SRTM with LiDAR attains a signal to noise ratio of 1; closely matching the divergence scale where the surface roughness of the land cover exceeds the roughness of the underlying terrain. As a result, the topographic expression of features at scales finer than 500 m may be corrupted by effects of land cover interaction with the radar signal. The 15″ resampling scale will effectively average elevations below the correlation scale where they approach the signal to noise ratio of the measurement process.

Fig. 1 shows a comparison of topography, population and night light for southeastern Asia. The locations of the megadeltas are labeled on the topography map. The lower panel of Fig. 1 shows a fused map of population density with night light change superimposed. Cities show up as white spots against a background of varying population density indicated as shades of gray. Color indicates change in night light brightness with warmer colors indicating increasing brightness.

2.4. Analysis

2.4.1. Bivariate population distributions

To quantify the relationship between population, elevation and coastal proximity, we follow the approach described by (Small and Cohen, 2004). Population counts were summed in1 km horizontal and 1 m vertical bins from coregistered population elevation and coastal proximity grids. Distance from coastline for each grid cell was computed using ArcGIS for each inhabited pixel (i.e. water mask applied) in the GPW4 grid. Spatial extents of the deltas are based on the Holocene transgression extents given by (Woodroffe et al., 2006) with grid coverages encompassing the full delta and surrounding areas. Each bivariate distribution is shown as a color image with warmer colors indicating greater numbers of people in the corresponding elevation/distance bin. Univariate marginal distributions of population as functions of coastal proximity and elevation are also given with cumulative population at and lower than the peak (most heavily populated) elevation labeled. To facilitate comparison among deltas, we also compute the bivariate cumulative distribution of population as a function of elevation and proximity for each delta. The diagonal cumulative giving total population within X vertical meters and X lateral kilometers of shoreline is shown along with the bivariate and marginal distributions for each delta and for the sum of all nine deltas.

2.4.2. Night light change maps

The dOLS + VIIRS composite product was produced by replacing the Value channel of a HSV-transformed tri-temporal (1992, 2002, 2012) OLS composite with a coregistered VIIRS monthly (June 2013) brightness composite then inverse transforming back to RGB space. Because the VIIRS dnb product has greater dynamic range and much reduced overglow, only the much brighter VIIRS pixels retain the color coded change information from the Hue and Saturation channels of the transformed OLS product. The inverse transformed combined product therefore retains the spatial detail and dynamic range of the VIIRS product and the decadal change information from the OLS product. While the resulting change map is not suitable for quantitative analysis, it does show the current spatial extents of the decadal change in much greater detail than is provided by the OLS product alone. Scatterplots showing temporal change in night light are derived from the dOLS + VIIRS composite to reduce the effects of overglow in the DMSP composites. For each delta, several night light brightness trajectory plots are included in an inset to illustrate year to year change in brightness from OLS. The color of each brightness trajectory plot corresponds to the color of the associated pixel on the dOLS + VIIRS composite. Warmer colors indicate brightening and cooler colors indicate dimming.

2.4.3. Population growth projections

Census data from the most current and a past census date are matched to a common set of boundaries. Annual growth rates are calculated for the matched data using a standard demographic formula:

$$r = \ln(P2/P1)/t$$

where r is the annualized growth rate, P1 is the population count at the time of the earlier census, P2 is the population count from the current census, and t is the number of years between population counts. These rates are used to interpolate and extrapolate population estimates based on the current census data and boundaries, often using a many-to-one relationship to transfer the rates from the less detailed (state/province or county equivalent) boundaries to the more detailed boundaries (enumeration areas, districts) that fall within them.

2.4.4. Spatiotemporal analysis of urban development networks

The evolving spatial structure of settlements (cities, towns villages, etc) on a landscape can be analyzed quantitatively as an evolving spatial network. To put the observed growth in lighted development occurring on the Asian megadeltas into the context of the rapid urban growth occurring throughout Asia, we conduct a spatiotemporal analysis of urban development networks using night light. The brightness of night light on the surface of the Earth is a continuous field. Maps of night light are useful because they show explicitly the intricate spatial patterns of the field reflecting the spatial structure of the settlements that produce the light. One of the primary observations immediately apparent in night light maps is the presence of interconnected spatial networks of lighted development. One way of conceptualizing the information contained in a continuous field is by quantifying its internal spatial connectivity structure. One useful framework for analyzing

fields with complex spatial structure is an approach based on spatial network analysis. Using this set of tools, a network is considered to be a composition of *nodes* connected by *links*. Each set of interlinked nodes is called a *component*. Taken together, a set of components forms a *network*. The nodes in many non-spatial networks are often interconnected to form a single "giant" component (Newman, 2010). However, segmentation of continuous geospatial fields generally results in a network with many components. For theoretical background on a network approach to continuous fields of land cover see (Small and Sousa, 2015).

To quantify the spatial network structure of a gridded continuous field like night light, a threshold brightness value is imposed which segments the continuous field into a binary map of pixels with data values greater than the threshold and pixels with values less than the threshold. Pixels exceeding the threshold become nodes in the network. Neighboring pixel nodes become connected into components (also called segments in this context). For more detail on the segmentation of continuous fields see (Small et al., 2011). In order to quantify the size distribution and network structure of lighted settlements at each time interval, we apply a brightness threshold to each OLS night light composite and compare the size distributions of the resulting contiguous components. As urban areas nucleate, grow and interconnect, the size distribution changes accordingly.

The size distribution of the components in a network can give information about its structure. Component size distribution for spatial networks of land cover are often heavy tailed (Small and Sousa, 2016; Sousa and Small, 2016). Plotting the sorted distribution of network components as a function of their ordinal rank (largest to smallest) on a log-log plot gives a clear and intuitive depiction of the size distribution of large numbers of components spanning a wide range of sizes. Rank size plots can be a convenient tool to explicitly display the information in heavy tailed distributions, and are typically shown on logarithmic axes because both the size range and numbers of components often span several orders of magnitude. This method of display is attractive because of its simplicity and minimum of assumptions regarding the inherent properties of the data.

Linearity of a rank-size plot on logarithmic axes is often interpreted to suggest the power law distribution as a likely candidate for the underlying process. A power law distribution is defined by a constant factor and an exponent. If observations are distributed according to a power law, the slope of the plot in logarithmic space can be directly converted to the exponent α by the following expression from (Li, 2002):

$$slope = -\frac{1}{\alpha - 1}$$

Power law statistics such as the best fit model parameters, the subset of the data most likely to follow this distribution, and confidence intervals can be computed using Monte Carlo methods and the Kolmogorov-Smirnoff nonparametric goodness-of-fit statistic. Methods to compute these statistics and example applications are given by (Clauset et al., 2009). Binned logarithmically, a rank-size distribution with a slope of −1 (and thus a power law exponent of −2) corresponds to a uniform distribution across scales (Small et al., 2011). Distributions with slopes less than −1 are dominated by large numbers of small components while distributions with slopes greater than −1 are dominated by small numbers of large components. The degree of linearity of the distribution indicates the degree to which it may conform to a scaling law between size and number of components.

In this analysis, we consider the process of urban growth on deltas in the context of evolving spatial networks of development. If the rank-size distributions of lighted settlement networks exhibit consistent scaling properties (as they have been observed to do elsewhere), this may imply some degree of predictability of future distributions of settlements. In addition, consistent scaling properties can provide powerful constraints with which to test urban growth models.

Using the procedure described by Small and Sousa (2015), we apply a brightness threshold to the 1992, 2002 and 2012 OLS night light composites, calculate the area of each spatially contiguous lighted area (city, town, village, etc), and compare the slope and linearity of the resulting logarithmic rank-size distributions across time and space. Power law fits are characterized by size cutoffs describing how much of the distribution is well-described as the lower limit is extended into the lower tail of the distribution. All distributions considered in this study had cut-offs smaller than 100 km^2. Cut-offs were determined using the same algorithm by choosing the minimum of the Kolmogorov-Smirnoff (KS) statistic for sets of points extending sequentially farther into the lower tail of the distribution. Statistical significance was estimated using a Monte Carlo approach to generate 1000 synthetic datasets and calculating the KS goodness-of-fit for each. Using this approach, large p values represent plausible power law fits. We follow the recommendation of Clauset et al. (2009) in presenting significant power law fits as those with $p > 0.1$.

It is important to remember that linearity of this rank-size distribution alone does not guarantee that it is a power law process, or exclude the possibility that other heavy tailed distributions may describe the data equally well – or even better (Clauset et al., 2009). In this analysis, we do not seek to draw any conclusions about the specific functional form of the underlying theoretical distribution from which the observations are derived. We merely use the statistical estimates of the best fit power law exponents as a convenient way to quantify the slope of the rank-size distribution and the range over which it may be considered linear. By comparing slopes of rank-size distributions of different regions at different times we can quantify the form of the spatial network of settlements and the ways in which it evolves through time.

3. Results

The results of the analysis of individual deltas are presented in Figs. A1 to A9 as a set of maps and population distributions for each delta with population distributions and elevation maps in the a) figure and VIIRS night light + SRTM shaded relief with dOLS + VIIRS change composite in the b) figure. Brief summaries of principal observations are given below.

3.1. Indus *Fig. A1*

Aside from the coastal city of Karachi, the population of the Indus delta is distributed more landward than the other deltas. Although the peak population occurs at an elevation of 11 m with only 4 million at lower elevations, the population is more broadly distributed with elevation than any of the other deltas. In part, this is due to the fact that most of the lower delta is sparsely populated with most of the population extending further north in the Indus river valley. Lighted development is largely confined to the Indus river valley in relatively close proximity to the main channel of the river. The Indus is the only delta with almost no urban expansion and many areas showing a significant decrease in night light brightness since 1992.

3.2. Ganges-Brahmaputra *Fig. A2*

The Ganges-Brahmaputra delta is, by far, the largest and most populous delta. With two densely populated megacities, Kolkata and Dhaka, numerous smaller cities and relatively dense rural populations extending far inland, the population is relatively evenly distributed with respect to coastal proximity. However, because of its large size and low gradient, it has a peak population at 9 m with 47 million living at lower elevations. Most of this population is displaced landward as most of the coastal zone is occupied by the Sundarban mangrove forest preserve. There is a noticeable disparity between population density and night light spanning the India/Bangladesh border with comparable densities in both countries but less extensive night light in many parts

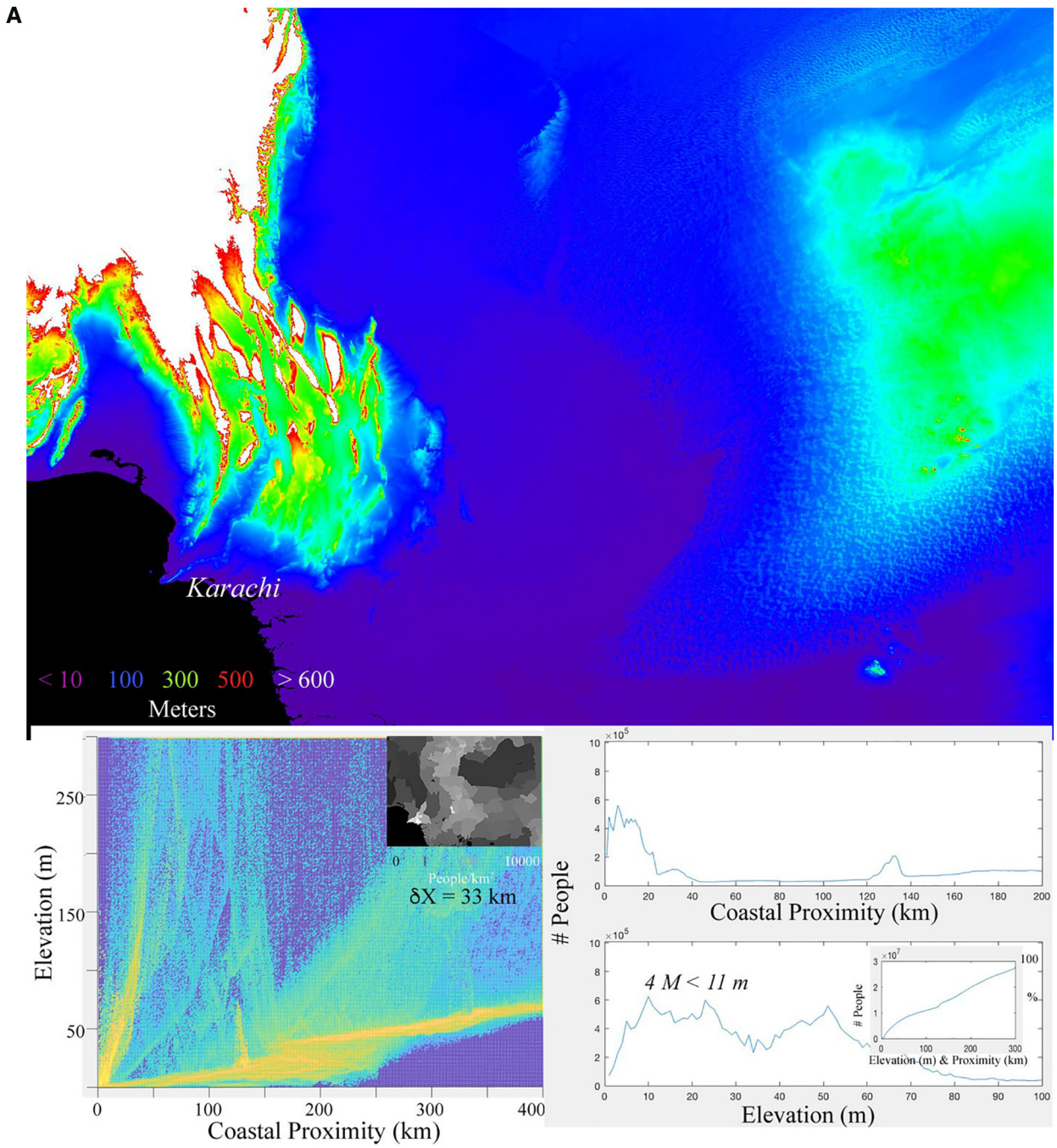

Fig. A1. a Population and topography on the Indus delta. Coregistered elevation (top) and population (inset), combined with distance from nearest coastline (proximity) yield a bivariate distribution of population as a function of elevation and coastal proximity (lower left). Marginal distributions (lower right) show the most populous elevation and distance. Inset cumulative shows total population along bivariate diagonal.
Fig. A1b Lighted development on the Indus delta. VIIRS dnb mean luminance superimposed on SRTM shaded relief (top) shows lighted development in context of topography. VIIRS dnb mean luminance from 2013 fused with OLS luminance change (bottom) shows little brightening (red & yellow) post-2002 with many areas apparently dimming (blue & green). Inset plots show example trajectories of brightness change for individual pixels. (For interpretation of the references to color in this figure legend, the reader is referred to the web version of this article.)

of Bangladesh. In both countries, most of the increase in lighted development has occurred at the periphery of the larger cities.

3.3. Irrawaddy Fig. A3

The Irrawaddy is, by far, the least populous delta with the smallest extent of lighted urban development and almost no urban growth. Like the Indus, it has a relatively small population of 4 million below its peak population elevation of 7 m, but this is due to the modest population densities (< 1000 people/km2) – even in Yangon. However, almost all of the population of the delta is below 20 m elevation.

3.4. Chao Phraya Fig. A4

Aside from the Chinese deltas, the Chao Phraya is the most extensively developed delta with considerable increases in lighted development throughout the delta, as well as along the coasts south of Bangkok. Both population and development are heavily concentrated

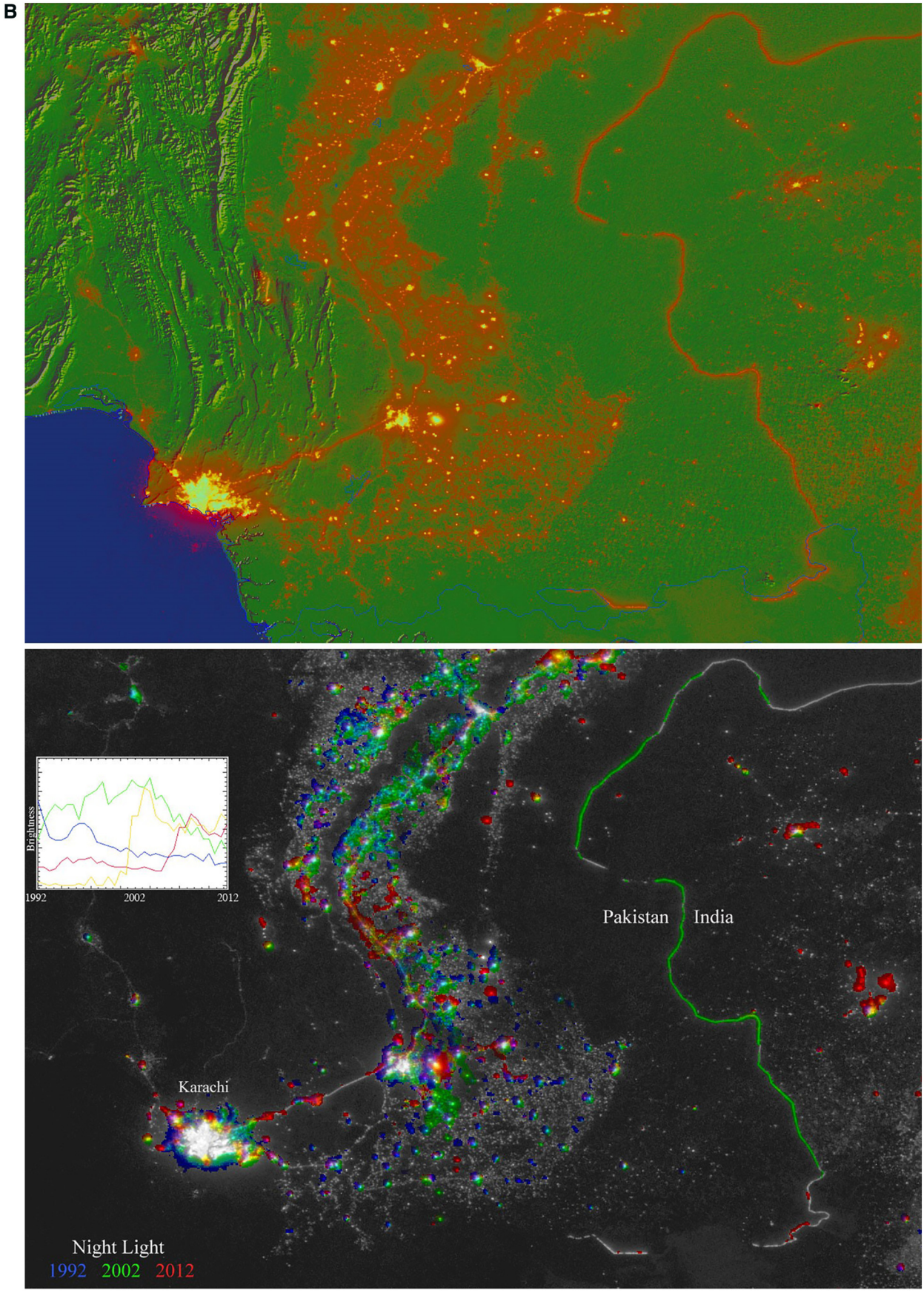

Fig. A1. (*continued*)

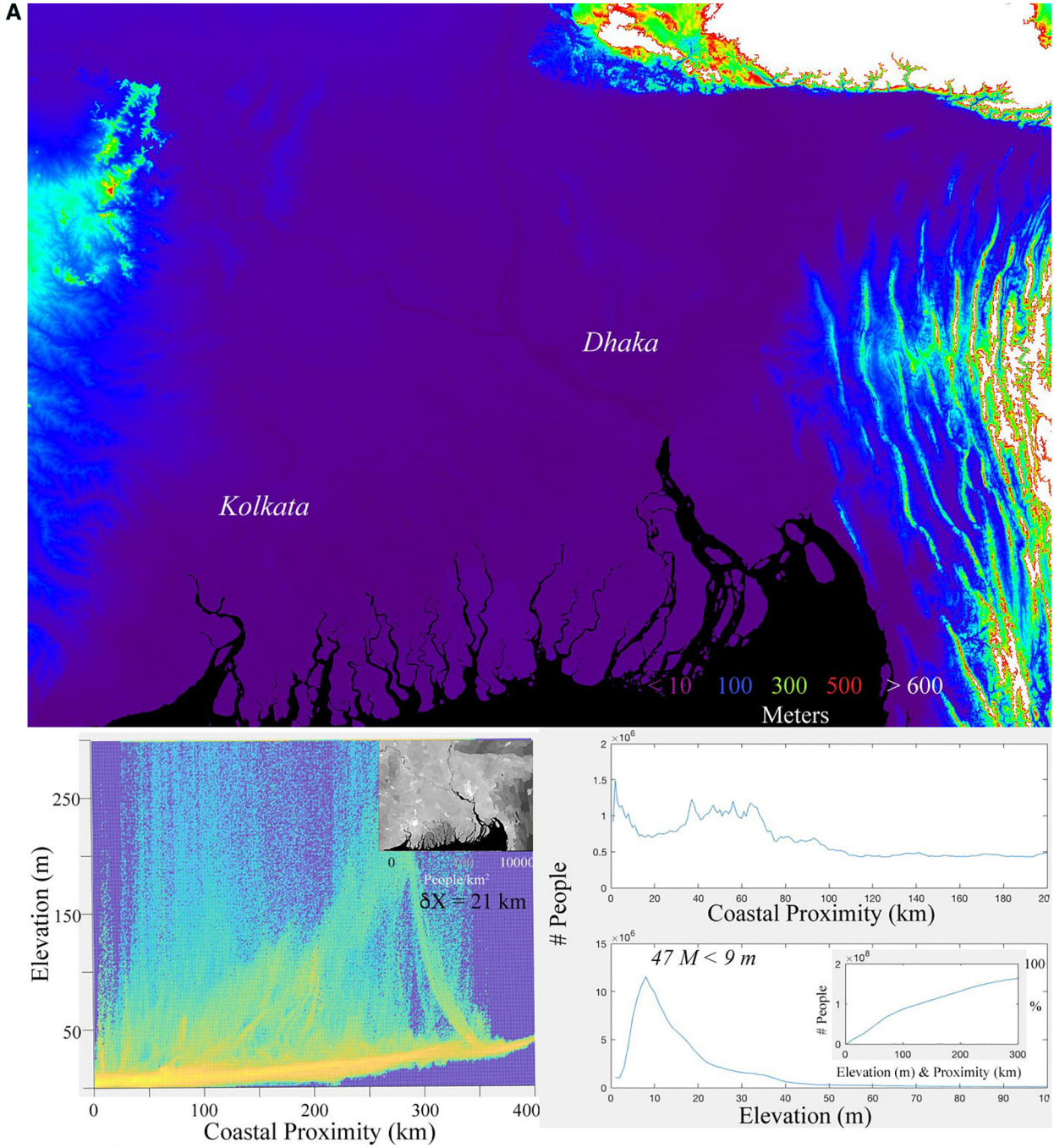

Fig. A2. a Population and topography on the Ganges-Brahmaputra delta. Coregistered elevation (top) and population (inset), combined with distance from nearest coastline (proximity) yield a bivariate distribution of population as a function of elevation and coastal proximity (lower left). Marginal distributions (lower right) show the most populous.elevation and distance. Inset cumulative shows total population on bivariate diagonal.
Fig. A2b Lighted development on the Ganges-Brahmaputra delta. VIIRS dnb mean luminance superimposed on SRTM shaded relief (top) shows lighted development in context of topography. VIIRS dnb mean luminance from 2013 fused with OLS luminance change (bottom) shows considerable brightening post-2002 over the entire delta. Peripheral brightening of cities, combined with infill development, results in interconnection of the spatial network of development. Inset plots show example trajectories of brightness change for individual pixels.

on the delta and coastlines with the surrounding mountains and plateaus sparsely populated and undeveloped. With a population of 9 million below a peak population elevation of 7 m, the population of the Chao Phraya is heavily localized in Bangkok, despite the extensive development of the entire delta.

3.5. Mekong Fig. A5

Because if its relatively low topographic gradient, the Mekong has a relatively large population of 12 million below a relatively low peak population elevation of 4 m. Most of the delta is sparsely illuminated but shows considerable increases in brightness of large areas around the periphery of Ho Chi Minh City, Tan An and Phnom Penh as well as at Phan Thiet on the coast to the north.

3.6. Red Fig. A6

The Red River delta is one of the smaller of the megadeltas and has

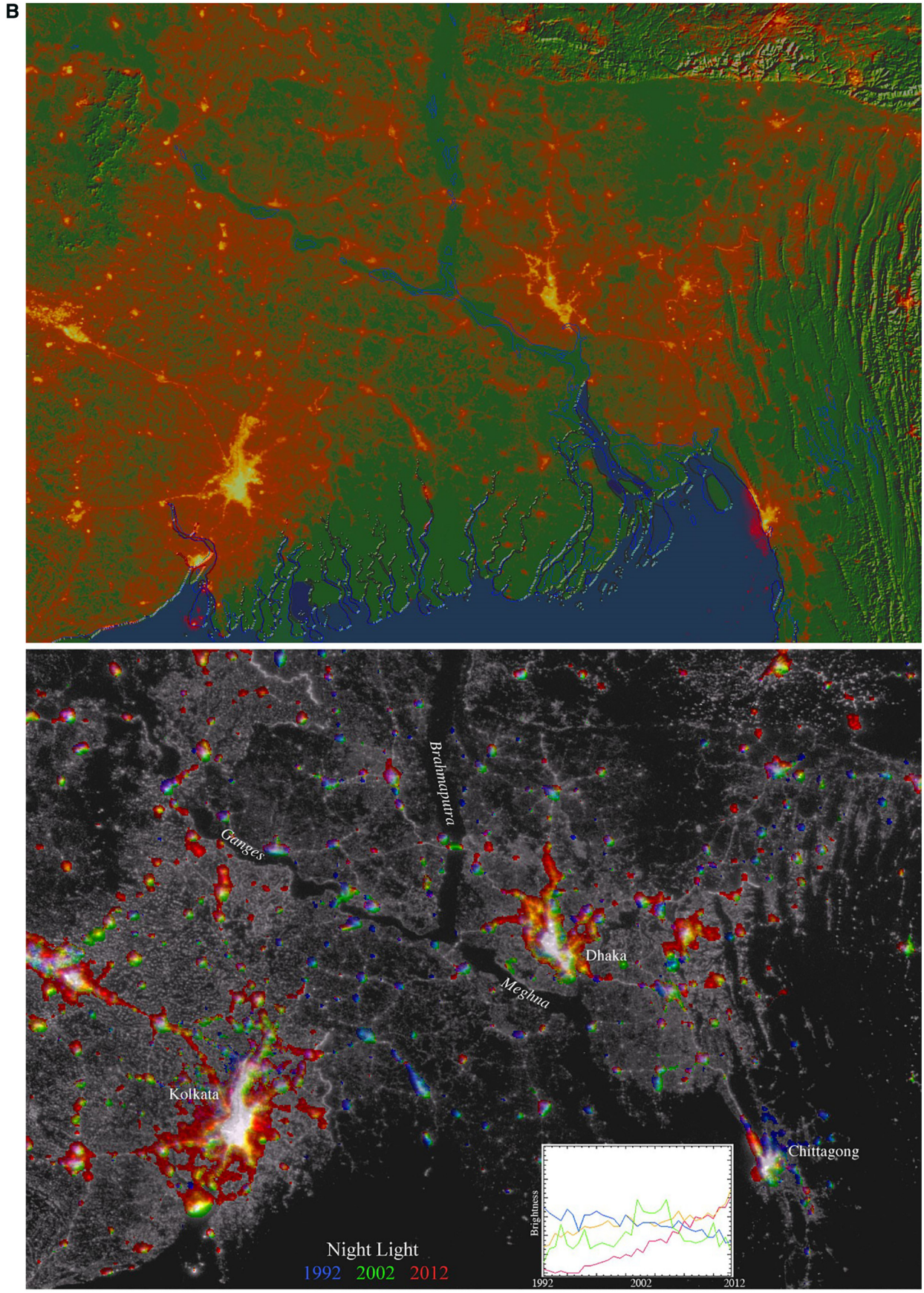

Fig. A2. (*continued*)

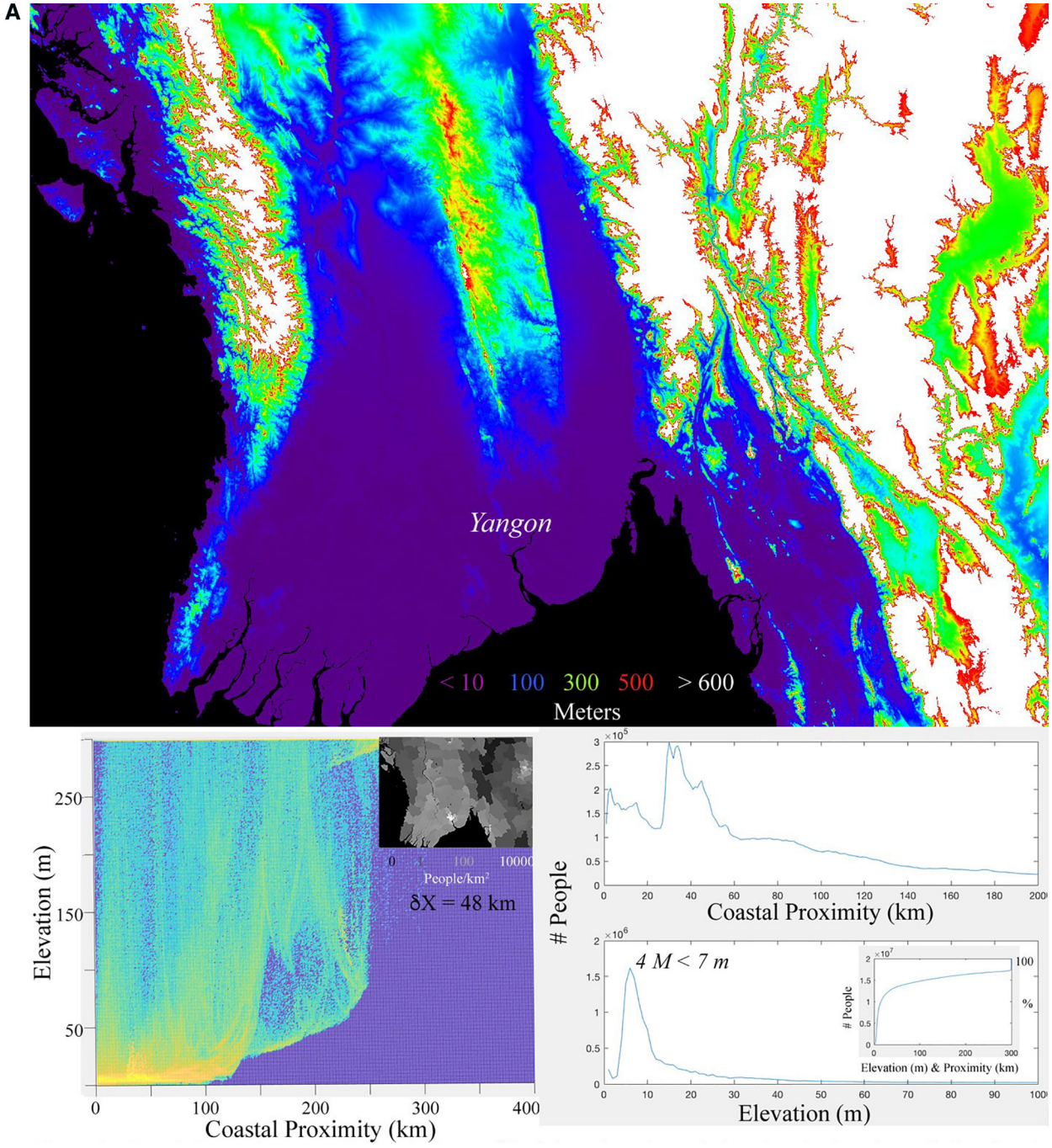

Fig. A3. a Population and topography on the Irrawaddy delta. Coregistered elevation (top) and population (inset), combined with distance from nearest coastline (proximity) yield a bivariate distribution of population as a function of elevation and coastal proximity (lower left). Marginal distributions (lower right) show the most populous elevation and distance. Inset cumulative shows total population on bivariate diagonal.

Fig. A3b Lighted development on the Irrawaddy delta. VIIRS dnb mean luminance superimposed on SRTM shaded relief (top) shows lighted development in context of topography. VIIRS dnb mean luminance from 2013 fused with OLS luminance change (bottom) shows almost no change on the delta post-1992, except around Yangon.

most of its population displaced landward away from the coast. As a result, it has a relatively small population of 5 million below its peak population elevation of 5 m. Nonethless, it is almost completely illuminated with considerable expansion of lighted development around both Hanoi and Haiphong. (For interpretation of the references to color in this figure legend, the reader is referred to the web version of this article.)

3.7. *Pearl* Fig. A7

The Pearl is the smallest of the Chinese megadeltas but has a large population therefore relatively high density. This, combined with its very low gradient, gives it a relatively high population of 7 million below a relatively low peak population elevation of 2 m. The Pearl River delta is heavily urbanized throughout the Macau-Guangzhou-Shenzhen-Hong Kong conurbation but has also experienced considerable expansion in lighted development along its entire periphery.

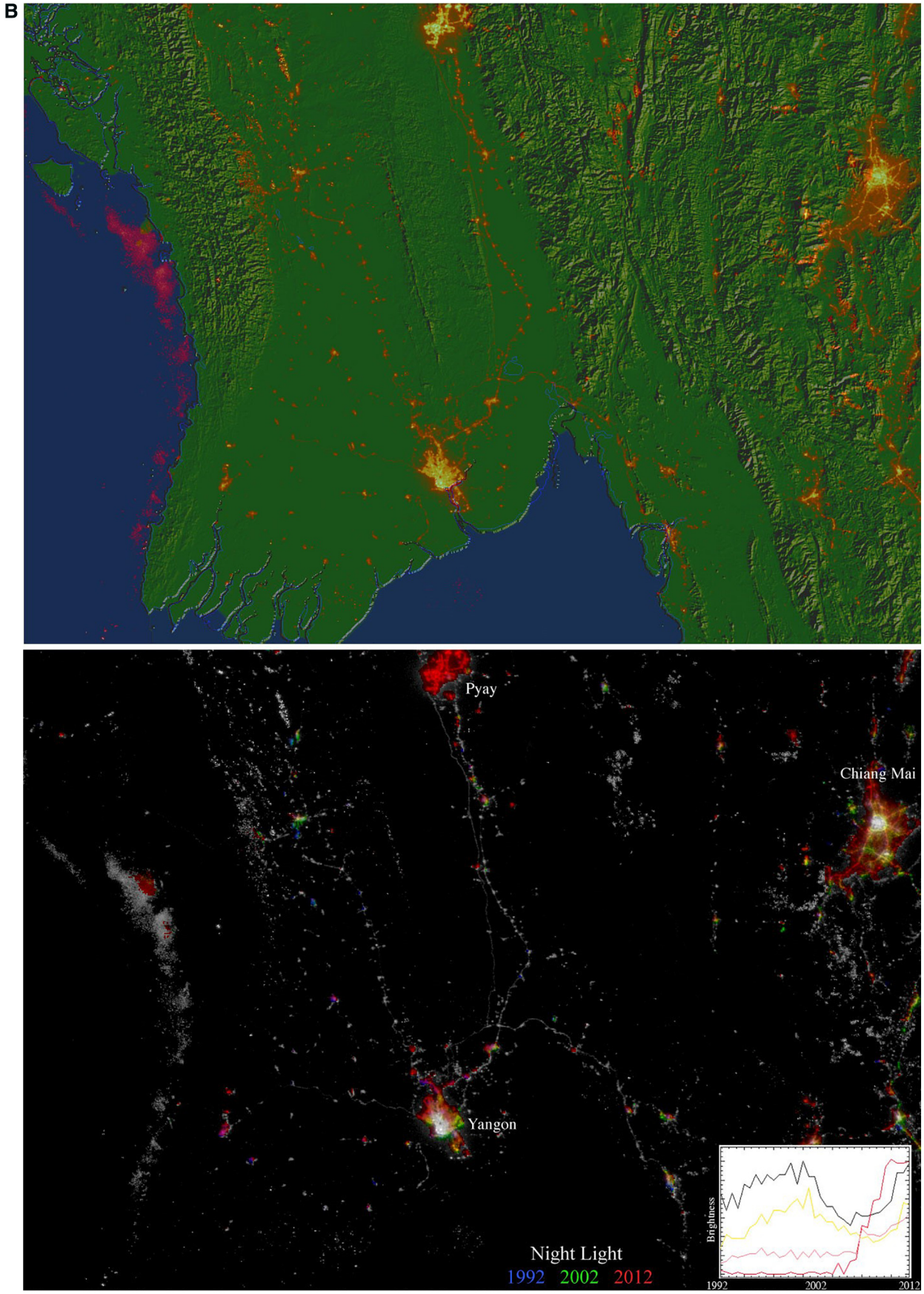

Fig. A3. (*continued*)

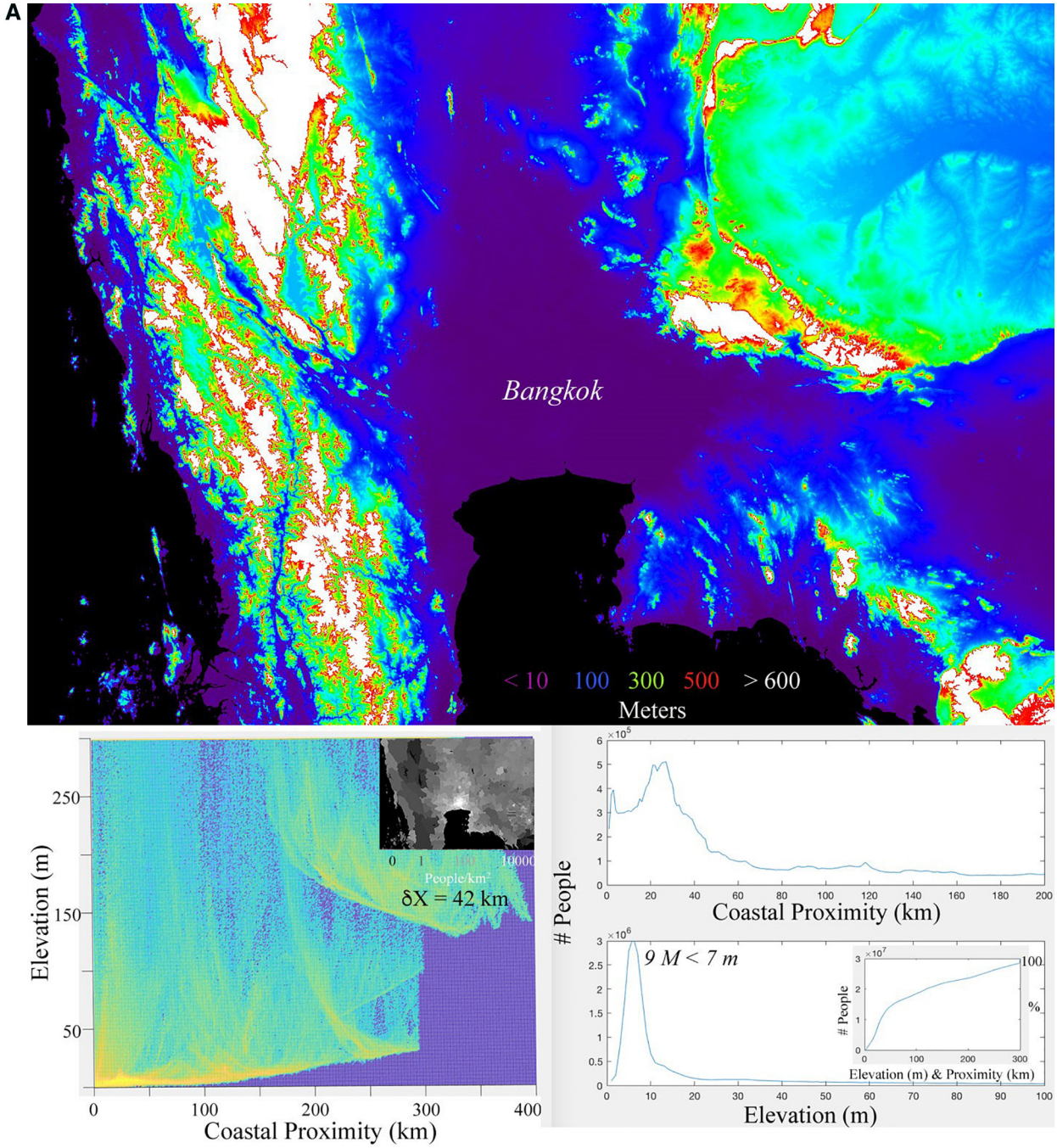

Fig. A4. a Population and topography on the Chao Phraya delta. Coregistered elevation (top) and population (inset), combined with distance from nearest coastline (proximity), yield a bivariate distribution of population as a function of elevation and coastal proximity (lower left). Marginal distributions (lower right) show the most populous elevation and distance. Inset cumulative shows total population on bivariate diagonal. Fig. A4b Lighted development on the Chao Phraya delta. VIIRS dnb mean luminance superimposed on SRTM shaded relief (top) shows lighted development in context of topography. VIIRS dnb mean luminance from 2013 fused with OLS luminance change (bottom) shows considerable brightening post-2002 over the entire delta and in coastal areas south of the delta. Peripheral brightening of cities combined with infill and corridor development results in interconnection of the spatial network. Lights in the Gulf of Thailand and Andaman Sea indicate dense fleets of fishing boats.

3.8. *Changjiang* Fig. A8

The Changjiang delta is the most densely populated and extensively developed of the Asian megadeltas. This, combined with its low gradient, gives it a considerable population of 24 million below its peak population elevation of 6 m. In addition to Shanghai, most of the delta, as well as the coast of Hangzhou Bay to the south, has experienced a great increase in lighted development since 2000.

3.9. *Huanghe* Fig. A9

The Huanghe delta is relatively large, and grades into the North China Plain to the southwest. Aside from the cities of Beijing and Tianjin, it has relatively modest population densities. Because of the topographic gradient it has only 14 million people below the peak population elevation of 9 m. Nonetheless, it is extensively developed with a large network cities of varying size. Like the other Chinese deltas, it has experienced considerable increase in lighted development

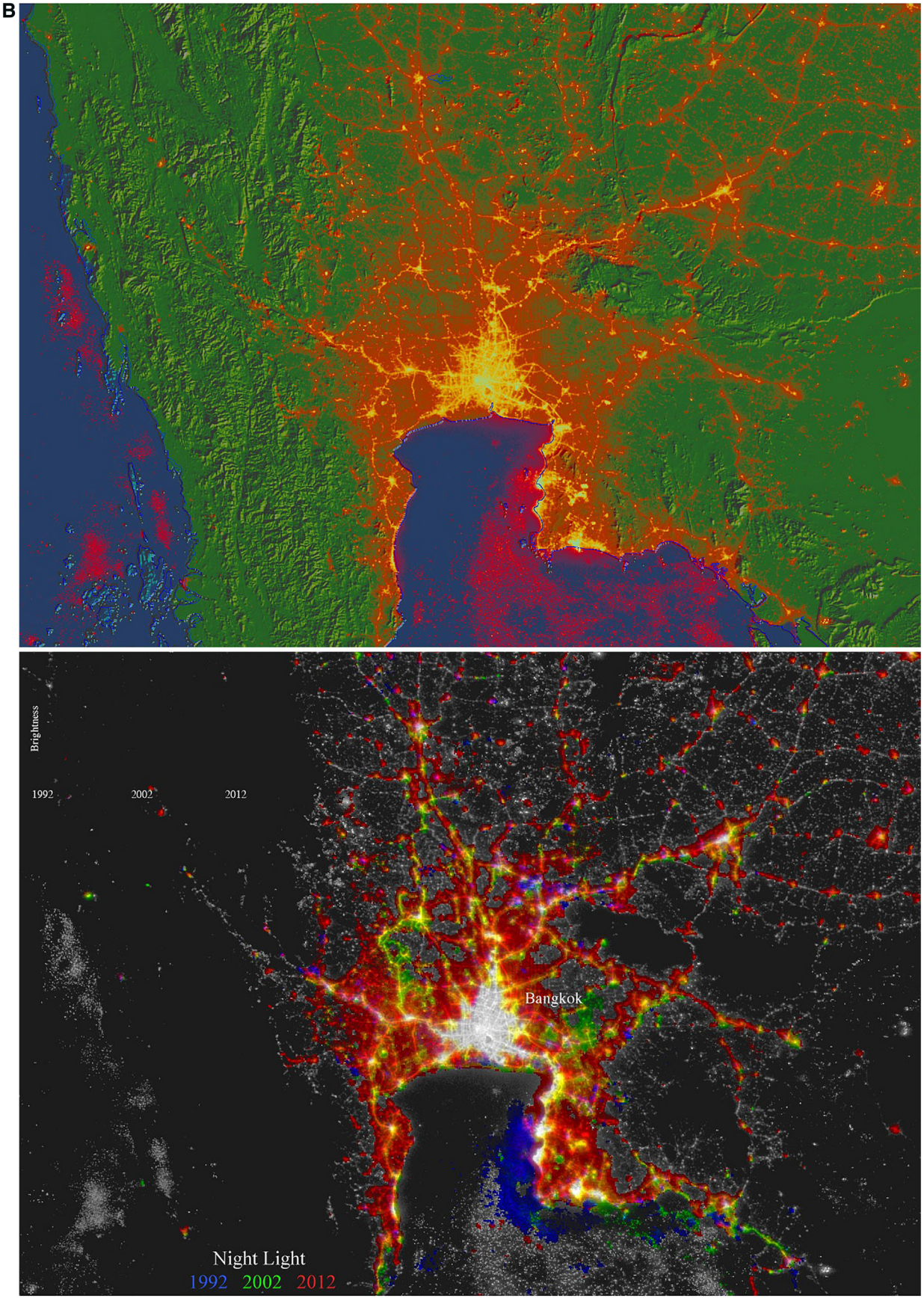

Fig. A4. (*continued*)

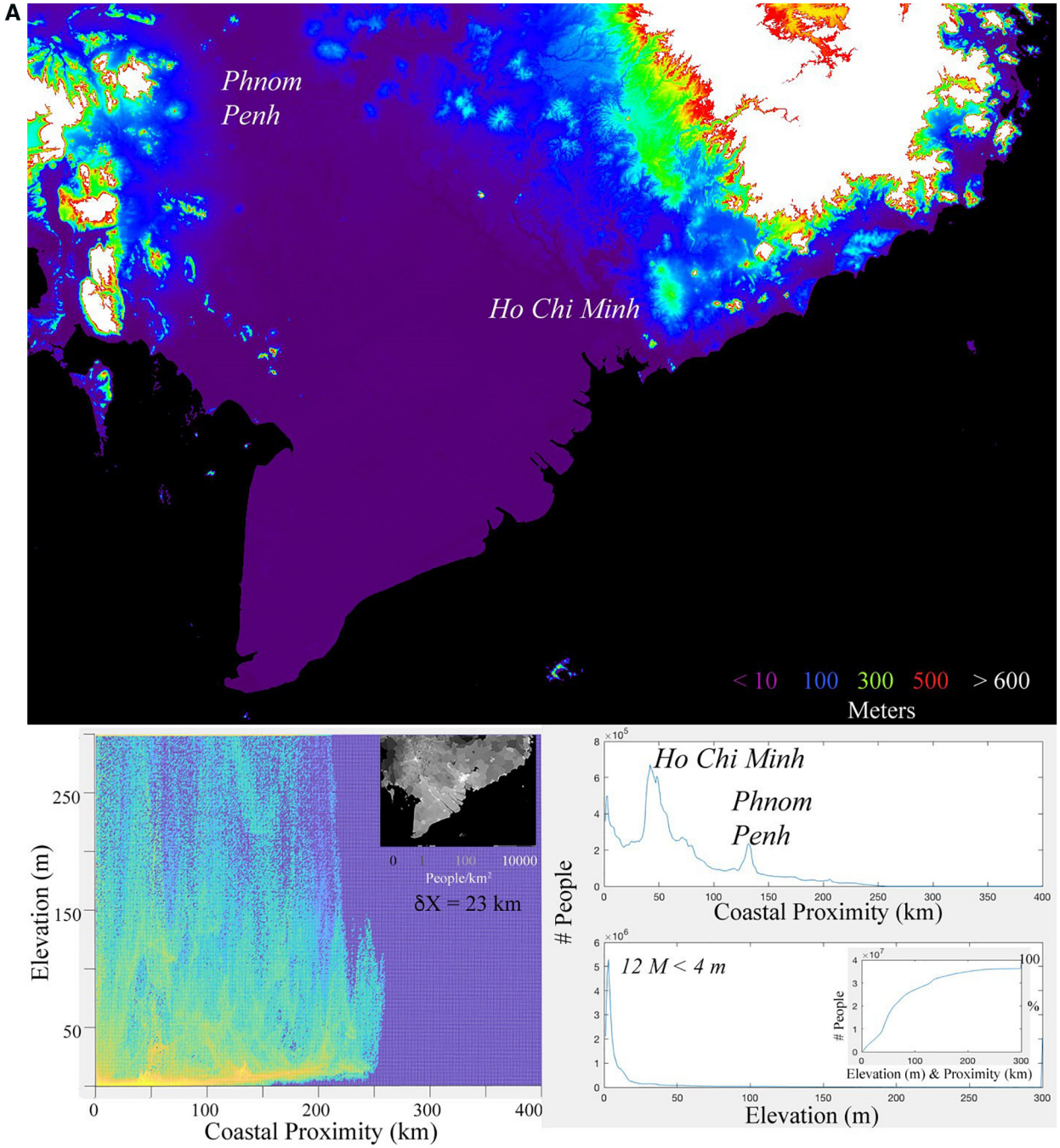

Fig. A5. b Population and topography on the Mekong delta. Coregistered elevation (top) and population (inset), combined with distance from nearest coastline (proximity) yield a bivariate distribution of population as a function of elevation and coastal proximity (lower left). Marginal distributions (lower right) show the most populous elevation and distance. Inset cumulative shows total population on bivariate diagonal.

Fig. A5b Lighted development on the Mekong delta. VIIRS dnb mean luminance superimposed on SRTM shaded relief (top) shows lighted development in context of topography. VIIRS dnb mean luminance from 2013 fused with OLS luminance change (bottom) shows considerable brightening post 2002 around the larger cities.

since 2000 with brightening occurring around the periphery of almost all settlements.

Comparison of the bivariate distributions reveals a common pattern of high populations at low elevations. The distributions differ primarily in their topographic gradient inland and in the extent to which population is concentrated near coastlines. All of the bivariate distributions show the largest number of people at the lowest elevation over the range of coastal proximities. In part, this is a function of the land area distribution, but it also reflects that fact that the highest population densities generally occur at the lowest elevation available.

The bivariate population distributions of all nine megadeltas can be summed to give an overall population distribution as shown in Fig. 2. The total distribution clearly shows the varying gradients of the individual deltas extending away from the coast, as well. The total distribution has a total of 174 million people below a peak population elevation of 7 m. The coastal proximity distribution shows a peak population at 3 km with 35 million people closer to the coasts, but with a relatively gradual decrease of population extending landward.

Because of the differences in spatial resolution of census data discussed above, we do not produce spatially explicit maps of population change for the megadeltas. However, we do provide projections of the aggregate population change within the study area of each delta, using

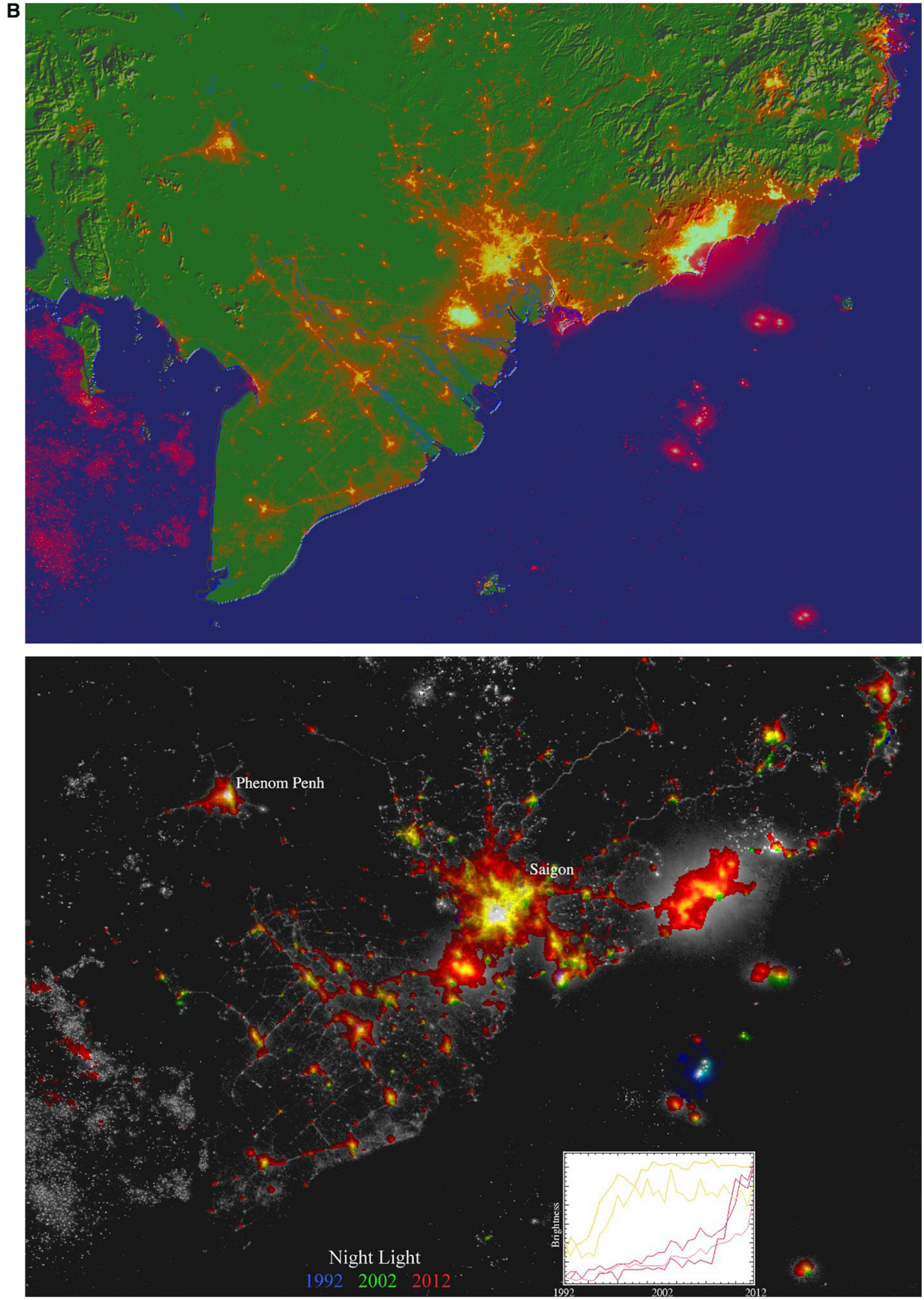

Fig. A5. (*continued*)

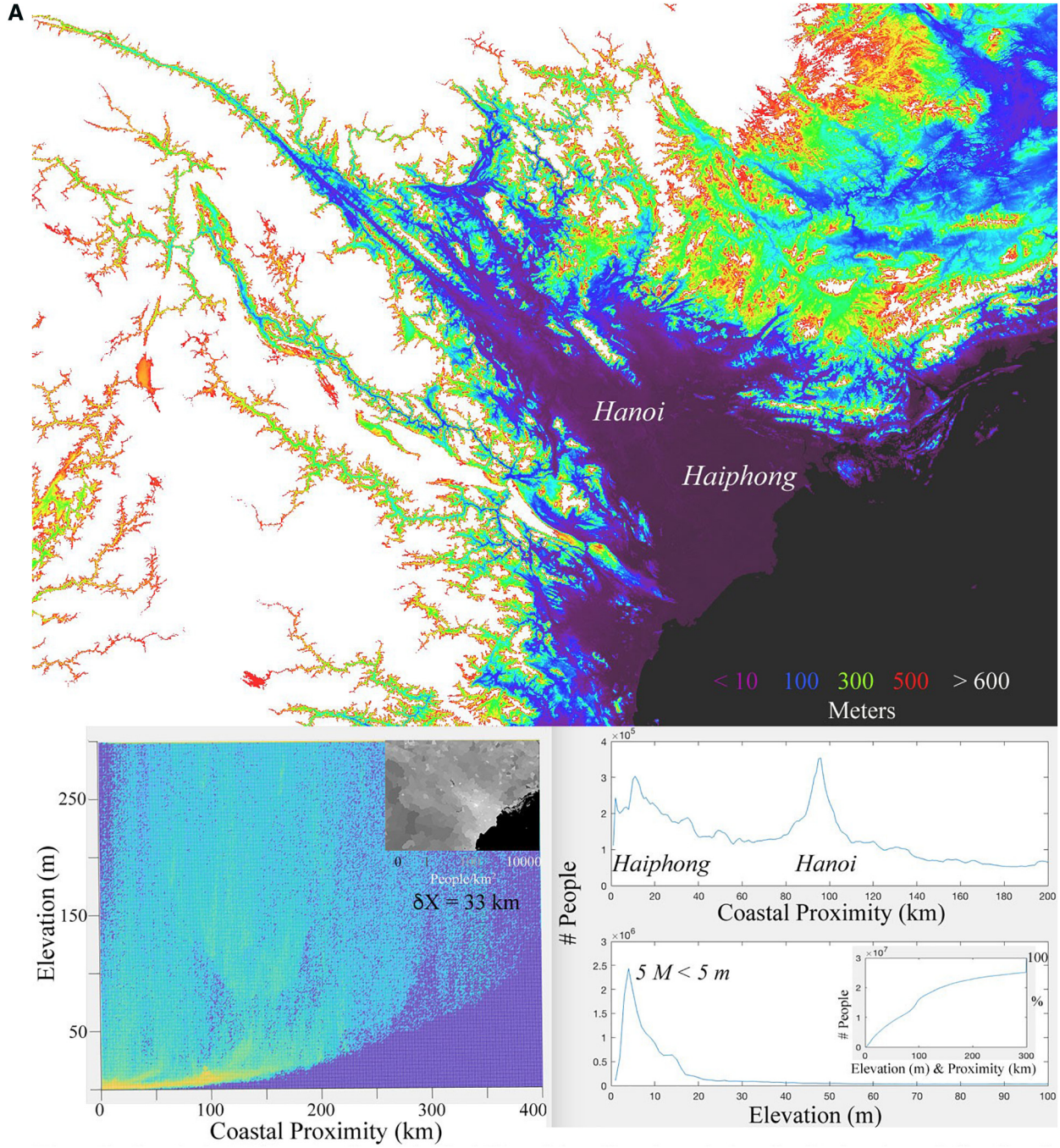

Fig. A6. a Population and topography on the Red River delta. Coregistered elevation (top) and population (inset), combined with distance from nearest coastline (proximity) yield a bivariate distribution of population as a function of elevation and coastal proximity (lower left). Marginal distributions (lower right) show the most populous elevation and distance. Inset cumulative shows total population on bivariate diagonal. (For interpretation of the references to color in this figure legend, the reader is referred to the web version of this article.)

Fig. A6b Lighted development on the Red River delta. VIIRS dnb mean luminance superimposed on SRTM shaded relief (top) shows lighted development in context of topography. VIIRS dnb mean luminance from 2013 fused with OLS luminance change (bottom) shows considerable brightening post-2002 around Hanoi and Hai Phong. Lights in Gulf of Tonkin show fleets of fishing boats. (For interpretation of the references to color in this figure legend, the reader is referred to the web version of this article.)

the procedure described above. These projections are summarized in the bar charts in Fig. 5. For comparison, the intercalibration of the DMSP-OLS night light composites does allow us to map changes in the location and spatial extent of lighted urban development at meaningful scales. Figs. 3 and 4 show changes in night light brightness between 1992 and 2012 as functions of coastal proximity and elevation for all of the megadeltas. The color of each bivariate distribution indicates the relative area that has experienced a given amount of brightening or dimming at each distance and elevation. Warmer colors correspond to greater areas. Both figures immediately show the marked difference in development with the South Asian deltas (Indus, Ganges-Brahmaputra, Irrawaddy) having the least lighted development, the Southeast Asian deltas (Chao Phraya, Mekong, Red) having moderate levels of development and brightening and the Chinese deltas having the greatest amount of lighted development and greatest extent of brightening. All deltas except the Indus show the greatest amount of lighted

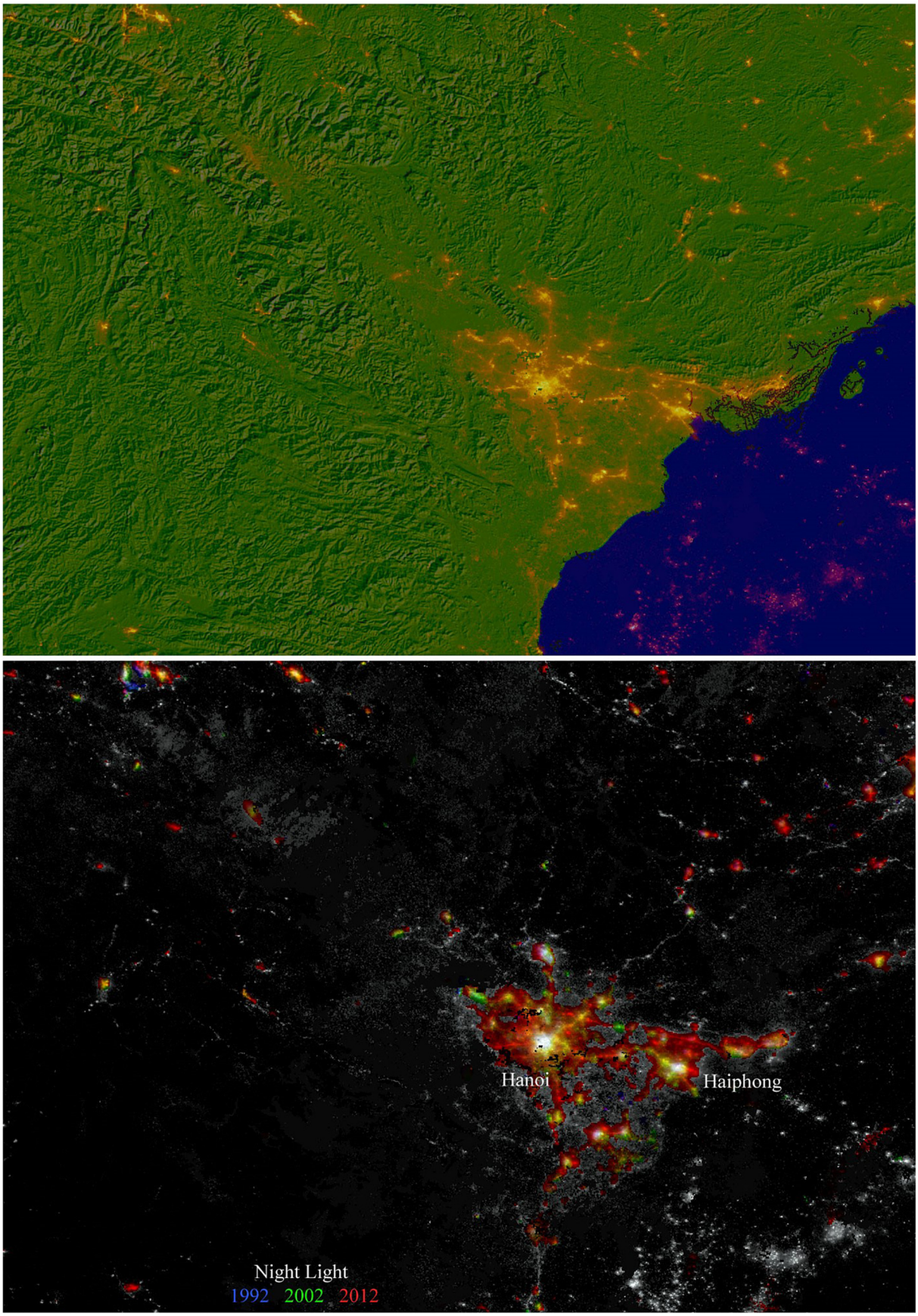

Fig. A6. (*continued*)

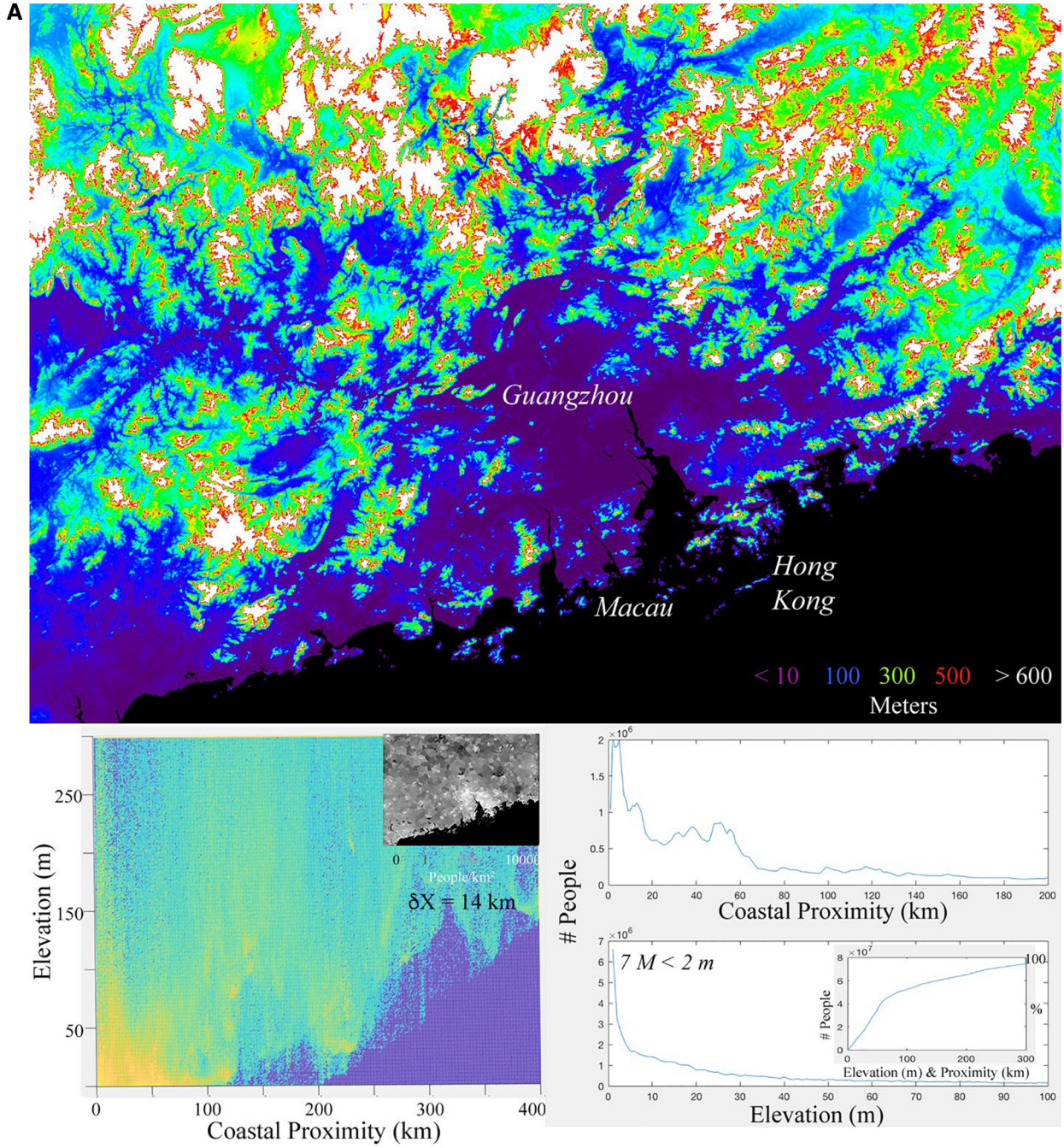

Fig. A7. a Population and topography on the Pearl River delta. Coregistered elevation (top) and population (inset), combined with distance from nearest coastline (proximity) yield a bivariate distribution of population as a function of elevation and coastal proximity (lower left). Marginal distributions (lower right) show the most populous elevation and distance. Inset cumulative shows total population on bivariate diagonal.

Fig. A7b Lighted development on the Pearl River delta. VIIRS dnb mean luminance superimposed on SRTM shaded relief (top) shows lighted development in context of topography. VIIRS dnb mean luminance from 2013 fused with OLS luminance change (bottom) shows considerable infill brightening post-1992 with more peripheral brightening post-2002. Both phases of development result in rapid interconnection of the spatial network.

development and greatest increase in brightness at low elevations (Fig. 3) but with increases occurring over a wide range of coastal proximities.

The rank-size distributions of lighted development in China and throughout Asia provide a complementary approach to understanding the growth of their networks. Fig. 6 compares rank-size distributions for China to those for all of Asia in 1994, 2004 and 2013 from the analysis of Small and Sousa (2015). The rank-size distributions for Asia are linear, maintaining slopes near −1 from 1994 to 2013. Although the Japan network was the largest in 1994, it fragmented in 2004 and was surpassed by both the Punjab and Huanghe networks in 2013. In comparison, China shows much more pronounced growth with network components of all spatial scales increasing in size over both time intervals. Even the differences among the three largest Chinese components are revealing. All three are approximately the same size in 1994 – but in 2013 now span almost an order of magnitude in size. Much of this is due to the rapid, expansive growth of the North China Plain component southward from Beijing to encompass the smaller cities of the plain, as well as the corridor of larger municipalities between Beijing and Xi'an. Much of this growth occurred after 2004, since at that

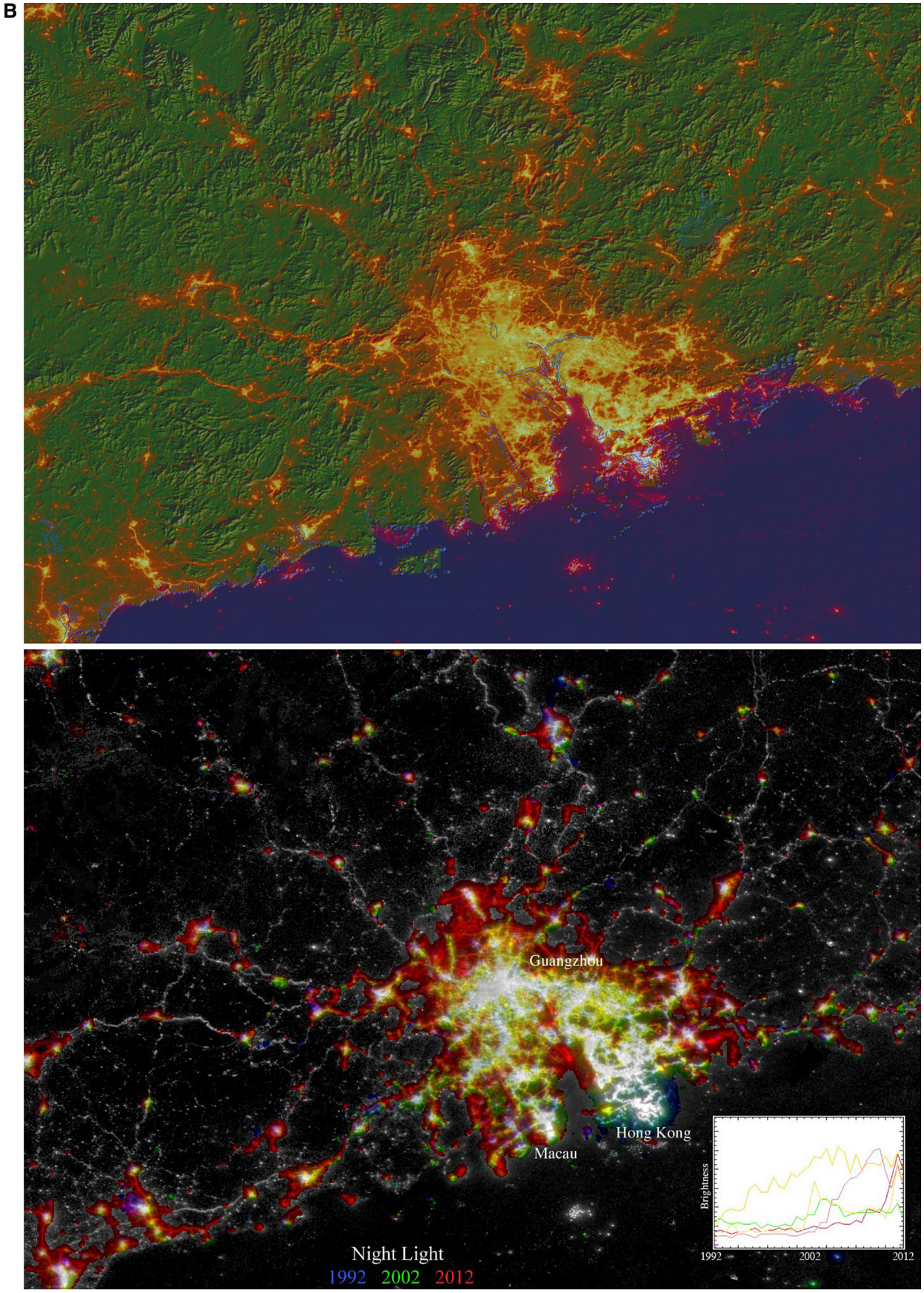

Fig. A7. (*continued*)

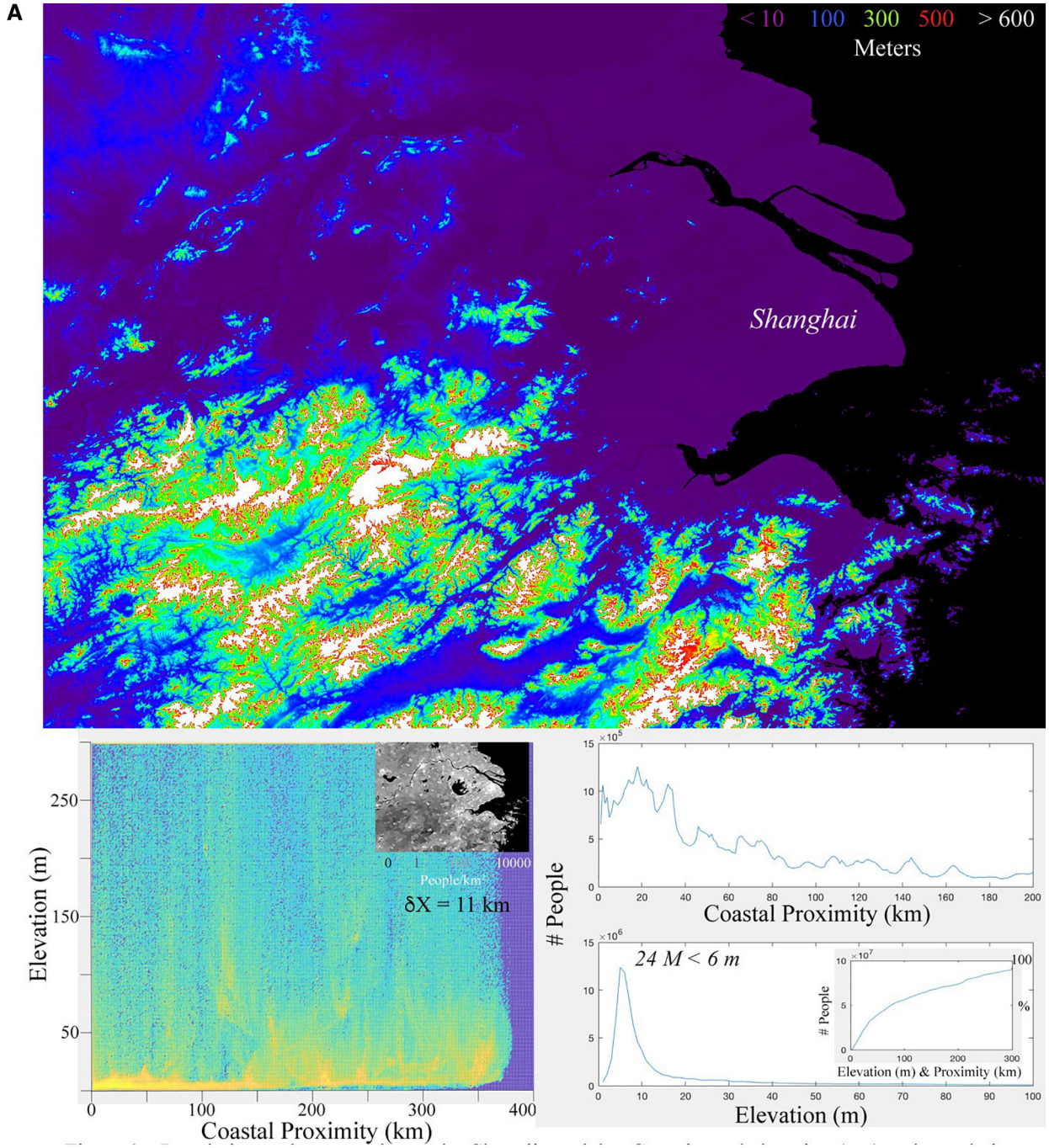

Fig. A8. a Population and topography on the Changjiang delta. Coregistered elevation (top) and population (inset), combined with distance from nearest coastline (proximity) yield a bivariate distribution of population as a function of elevation and coastal proximity (lower left). Marginal distributions (lower right) show the most populous elevation and distance. Inset cumulative shows total population on bivariate diagonal.

Fig. A8b Lighted development on the Changjiang delta. VIIRS dnb mean luminance superimposed on SRTM shaded relief (top) shows lighted development in context of topography. VIIRS dnb mean luminance from 2013 fused with OLS luminance change (bottom) shows some peripheral brightening around the larger cities post-1992, followed by considerable infill brightening post-2002 over the entire delta. More isolated cities in the mountains to the south also show brightening post-2002, with more connection along corridors of development.

time the area of the Changjiang Delta component actually slightly surpassed it. Finally, the nucleation of new lighted settlements at the bottom of the distributions has steadily increased for China. This is expected to be the result of increasing rural electrification, not necessarily the formation of new villages. As expected, all the rank-size distributions in Fig. 6 roll off at the smallest segment sizes because of these components approach the sensor detection limit. However, the persistence of slopes near −1 suggests consistent scaling properties of the Chinese and Asian networks at multiple spatial scales over the course of two decades.

4. Discussion

The spatial resolution of the population density and night light brightness data used in this analysis allow for a more spatially explicit analysis of the relationship between the morphology of each delta and the distribution of its human inhabitants and development. In comparison to earlier global analyses, the intersection of the anthropogenic

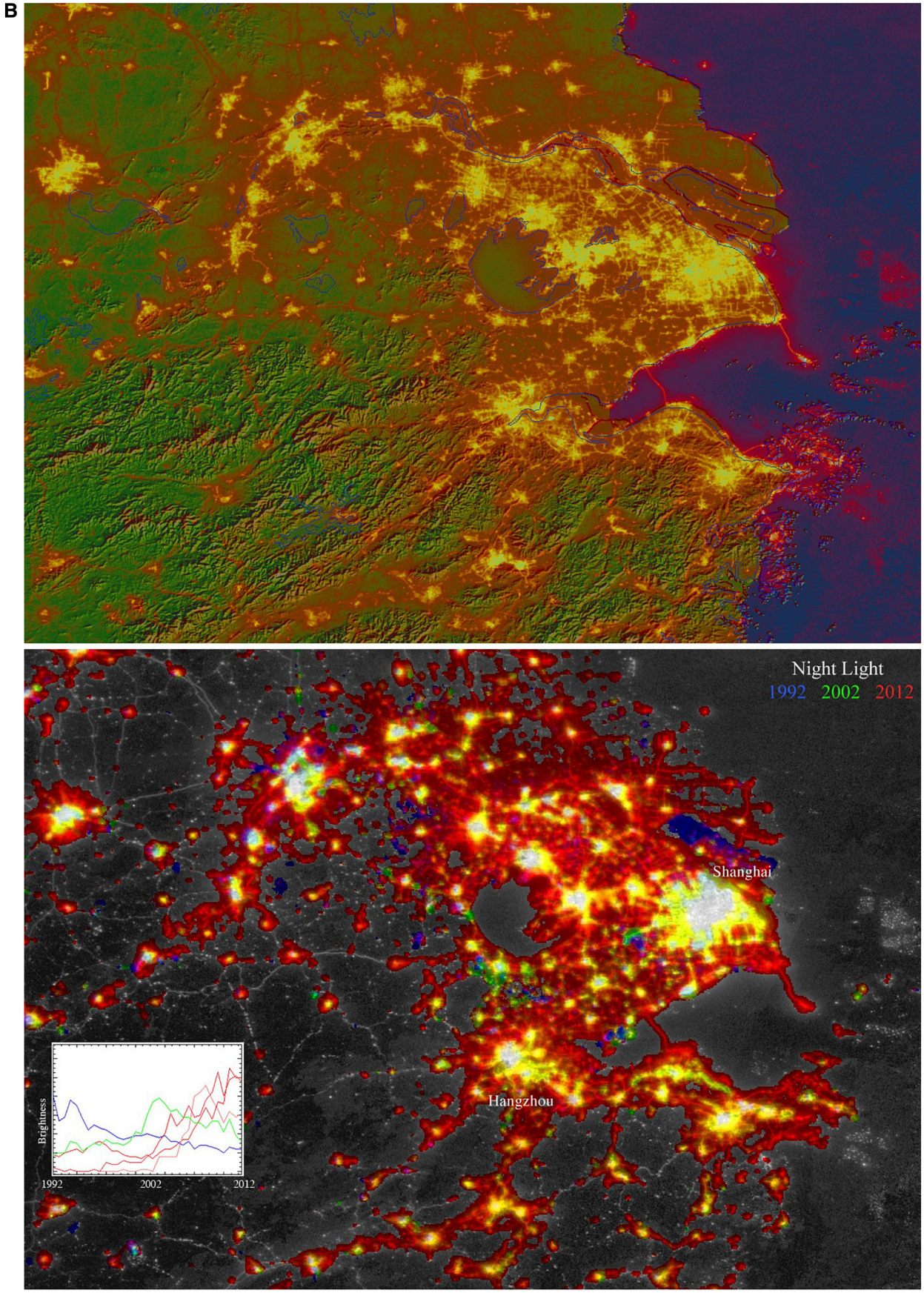

Fig. A8. (*continued*)

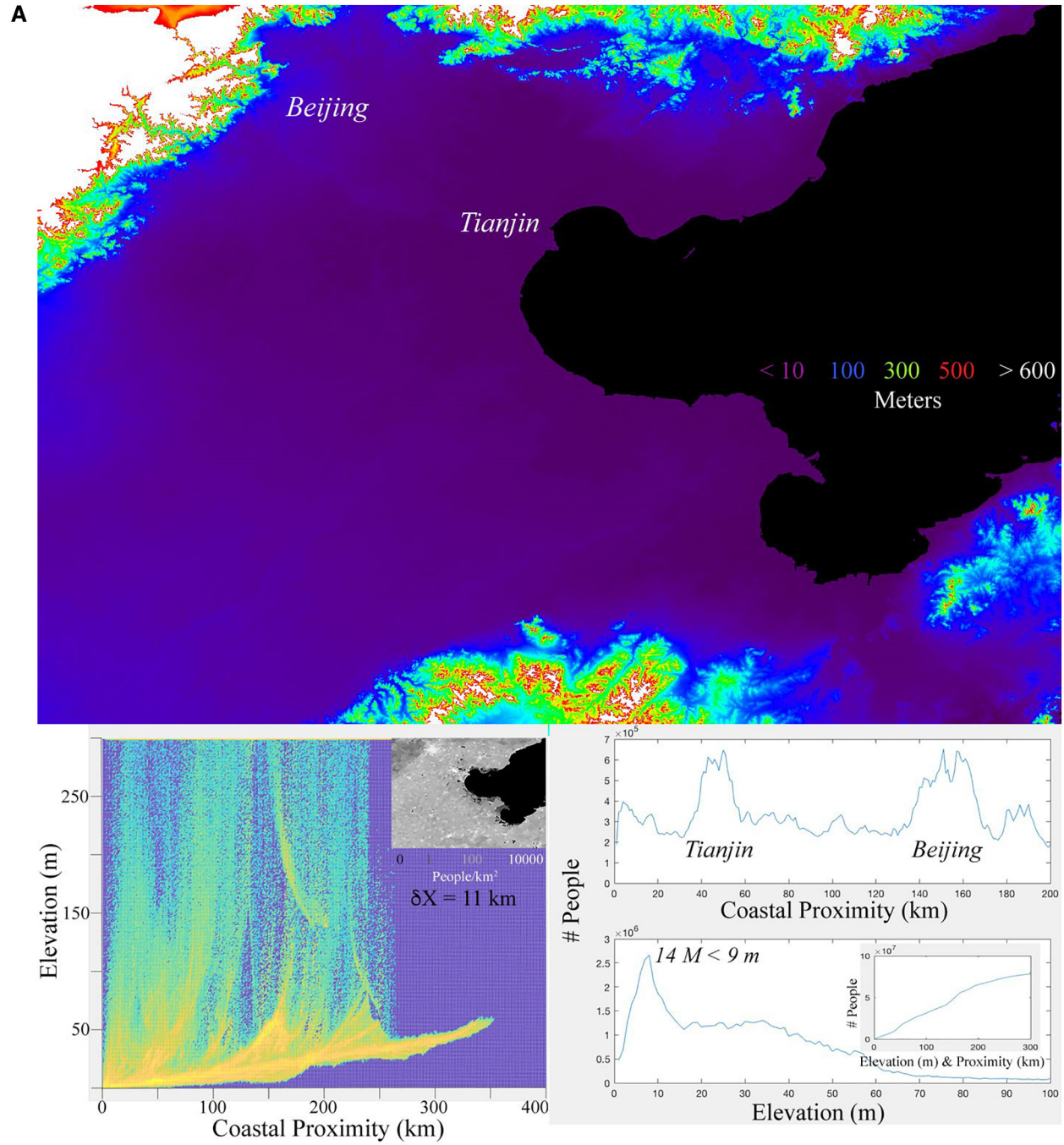

Fig. A9. a Population and topography on the Huanghe delta. Coregistered elevation (top) and population (inset), combined with distance from nearest coastline (proximity) yield a bivariate distribution of population as a function of elevation and coastal proximity (lower left). Marginal distributions (lower right) show the most populous elevation and distance. Inset cumulative shows total population on bivariate diagonal.
Fig. A9b Lighted development on the Huanghe delta. VIIRS dnb mean luminance superimposed on SRTM shaded relief (top) shows lighted development in context of topography. VIIRS dnb mean luminance from 2013 fused with OLS luminance change (bottom) shows considerable peripheral brightening post-2002 around cities of all sizes. Lights in the Bohai Sea correspond to both fishing boats and offshore oil and gas production.

and geodynamic characteristics of individual deltas allow each to be considered in the context of its specific combination of morphology and anthropogenic land use. While we hope that these maps and data will be informative for local and regional specialists considering specific scenarios on their delta of interest, we can also draw some more general conclusions about two specific aspects of anthro-deltaic processes in the context of earlier studies. The relationship(s) between delta morphology and land use have implications for the future, should development on each of these deltas continue on its present trajectory over the past 25 years. The relationship between the current distribution of population and the low elevation coastal zone has related implications for potential exposure to coastal and flood hazards.

4.1. Geomorphology and land use

Whereas the inspirational work of Woodroffe et al. (2006) focused primarily on the natural processes operating on the Asian megadeltas, this analysis focuses on distribution of population distribution and evolution of lighted development on these deltas. Comparison of the bivariate distributions of population shows very different relationships

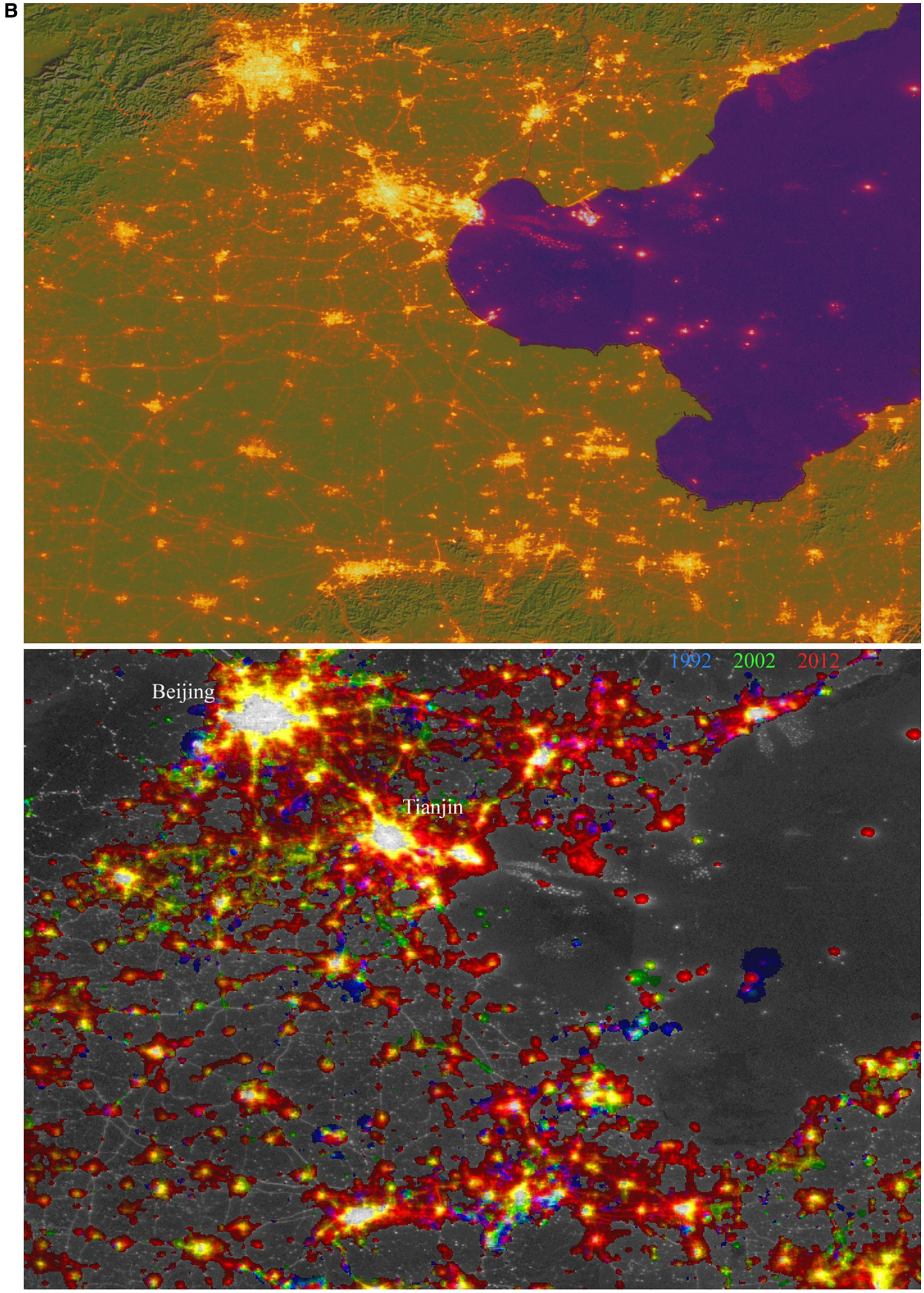

Fig. A9. (*continued*)

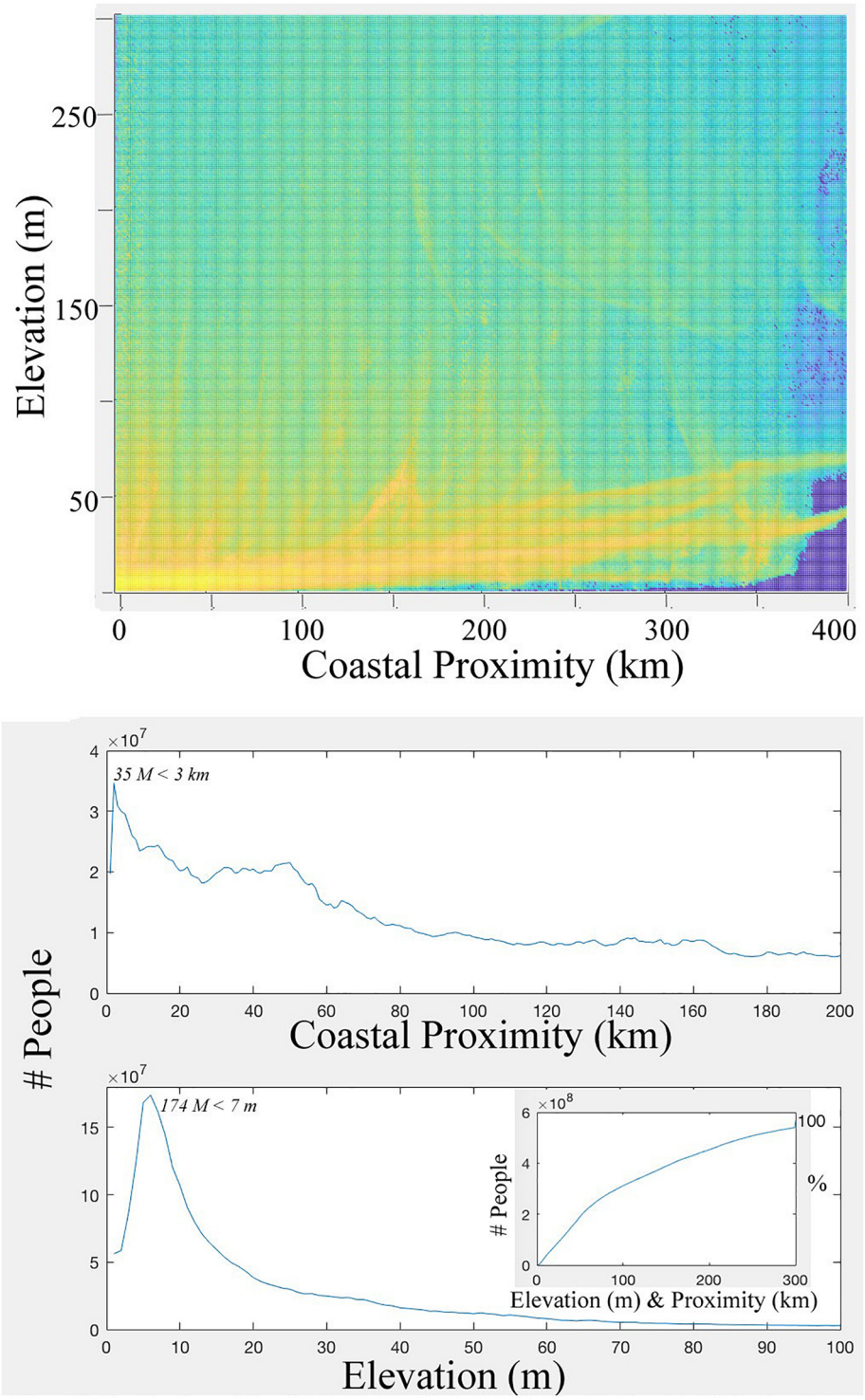

Fig. 2. Combined population distribution for all nine Asian deltas. The bivariate distribution shows different elevation gradients for different deltas as distinct ridges of population increasing in elevation with distance from coastline. The marginal distributions show clear population peaks at elevations < 7 m and proximities < 3 km. Inset cumulative shows total population on bivariate diagonal.

between the populations and the deltas they inhabit. The populations of the South Asian deltas (Indus & GBD) are less urban and more evenly dispersed with respect to coastal proximity and elevation, while the populations of the Southeast Asian deltas (Irrawaddy, Chao Phraya, Mekong, Red) are concentrated within 60 km of the coastline. The three Chinese deltas provide examples of both patterns – but with much faster recent rates of development. The obvious reason for the difference is related to the geomorphology of the deltas and their watersheds, with the presence of uplifted highlands and rougher terrain limiting the areas suitable for agriculture. However, geomorphology also constrains the form of urban development networks, thereby creating competition between urban and agricultural land use for both space and water.

Observed differences in the form and rate of urban growth among deltas highlights the differing impact of socioeconomic factors and the competition between agriculture and urban development in different settings. The impact of urban development on the loss of potential

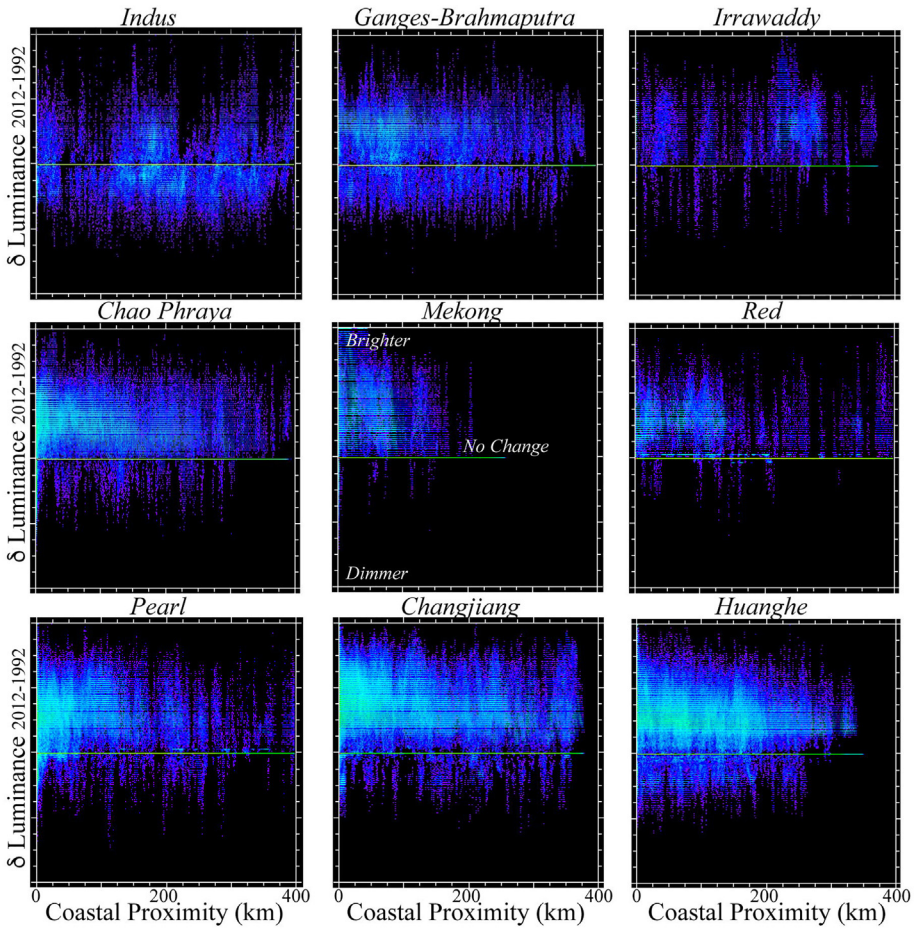

Fig. 3. Change in lighted development and coastal proximity. Bivariate distributions of land area as function of coastal proximity and change in luminance between 1992 and 2012. All deltas except the Indus have far more area brightening than dimming. Greatest increases in luminance generally occur nearest the coastline but moderate increases occur over a wide range of distances from the coast.

agricultural land in the USA has been estimated as equivalent to the caloric requirement of 6% of the US population by (Imhoff et al., 2004). However, the analysis of the USA includes mostly non-deltaic agricultural areas, often without the spatial constraints imposed by deltas. The study of (Jiang et al., 2015) estimated a loss of 0.137 TgC of Net Primary Productivity (NPP) from the combined loss of forest and agricultural land to urban growth on the Pearl River Delta between 2000 and 2010. An urban growth model was used by (d'Amoura et al., 2017) to project potential loss of cropland to urban development worldwide, projecting a total loss of 16 to 21 Mha for all of Asia. Of the deltas considered here, the most obvious loss of cropland to recent urban development is the rapid and extensive development of the Chinese deltas. Although agricultural land use continues to be interspersed within the development on the Chinese deltas, this development does come at the expense of reduced area available for agriculture on some of the most fertile and well-watered soils available.

4.2. Implications for hazards

While the data used in this analysis do not provide a sufficient basis for detailed hazard assessments, they do illustrate the relationship between population and delta morphology at levels of detail not previously available, as well as temporal evolution of development in a variety of geomorphic and socioeconomic settings. Even with advances in phone-based studies of call/text volumes and individual mobility, detailed mapping of population distribution remains challenging. However, increases in the spatial resolution of night light sensors, and their integration into multi-sensor fusion products will continue to provide increasingly detailed maps of infrastructure and development. Combined with more detailed DEMs, the analytical methods illustrated here can be extended to higher spatial resolution to inform more detailed hazard assessments.

As demonstrated by earlier continental-scale analyses (e.g.,(Small and Nicholls, 2003),(McGranahan et al., 2008)), coastal zones are often the locus of countries' largest cities, although it is not clear whether these coastal cities are necessarily the fastest growing (Balk et al., 2009). The delta-specific population growth rates given in Fig. 14 are generally greater than the corresponding country growth rates but some inland areas may still be growing faster. Regardless, it is clear from Figs. 12–14 that delta populations are growing at considerable rates and that urban expansion is occurring rapidly over the past two decades. This has implications for coastal hazard because, as demonstrated by Ericson et al. (2006), anthropogenic processes often contribute more than eustatic sea level rise than the effective sea level rise that actually impacts coastal zones.

Quantifying the spatiotemporal evolution of urban networks of development throughout Asia provides a context for urban growth on the megadeltas relative to other geomorphic settings. This is particularly apparent on the more rapidly developing Chinese deltas as their networks have now grown beyond the deltas and become interconnected with much larger regional networks. The fact that the Huanghe Delta + North China Plain network is now the largest in Asia, and may soon connect with the Chiangjiang Delta network underscores the importance of the development on the Chinese deltas. In contrast, the corridor structure of network development in India does not appear to be driven by development on the deltas (Small and Sousa, 2015).

4.3. Comparison to earlier analyses

The higher spatial resolution of the GPW4 population grids allow the relationship between population, elevation and coastal proximity in different deltaic settings to be quantified in much greater detail than

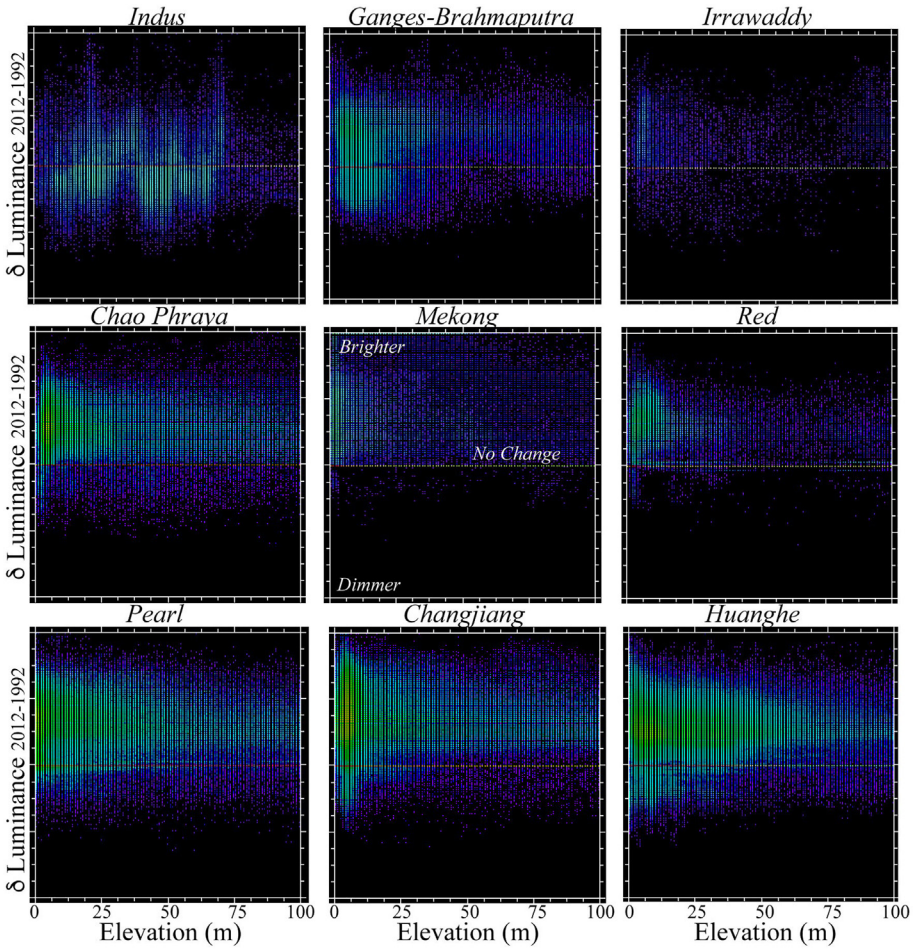

Fig. 4. Change in lighted development and elevation. Bivariate distributions of land area as function of elevation and change in luminance between 1992 and 2012. All deltas except the Indus have far more area brightening than dimming. Greatest increases in luminance generally occur at elevations < 25 m and diminish rapidly upward.

previously possible. For the most densely populated Chinese deltas, the 11–14 km mean resolution of the census administrative units allows for the distribution relative to the topography of the delta to be seen clearly in the a) figures. The lower resolution of the South Asian countries introduces more uncertainty, but the grand scale and low gradient of the Ganges-Brahmaputra delta offsets this uncertainty somewhat. The bivariate distributions in the a) figures clearly show the mean gradients relative to coastal proximity as the envelope of the overall population

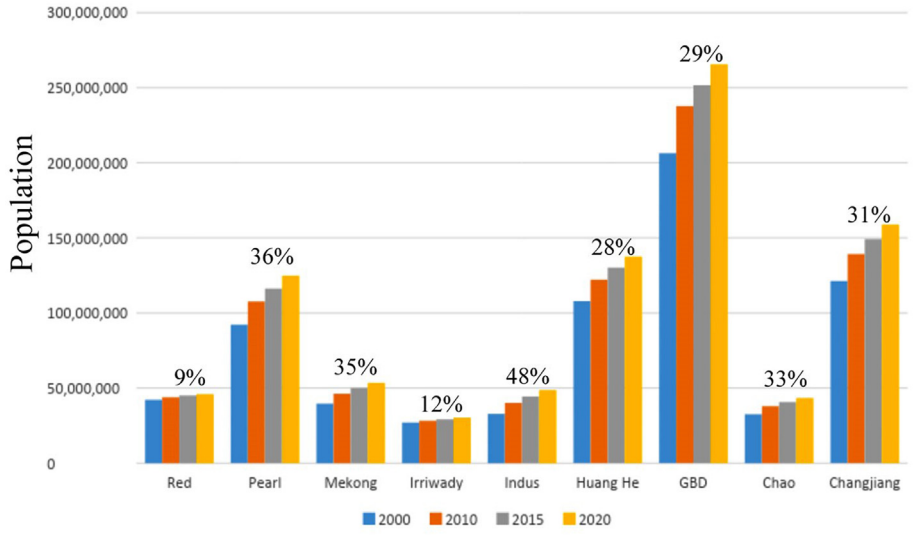

Fig. 5. Past and projected population growth on the Asian megadeltas and surrounding areas. Total population given within the bounds of each delta study areas. Projections for 2015 and 2020 are based on regional growth rates between 2000 and 2010.

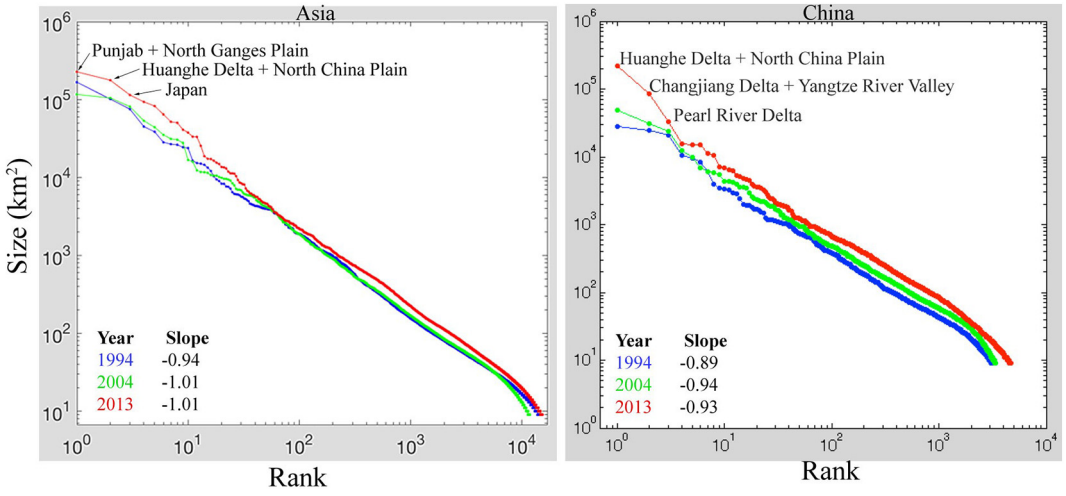

Fig. 6. Growth of spatial networks of night light throughout Asia and in China from Small and Sousa (2015). Rank-size distributions of contiguous networks maintain slopes near −1 with slight increases as networks grow. Parallel upward progression of rank-size distributions indicates that network components of all sizes are nucleating, growing and linking at comparable rates. Since 2004, the Punjab and Huanghe networks have grown to surpass the Japan network in size. Within China, the three megadelta networks are the largest. In 1994, the Huanghe and Changjiang were smaller than predicted by the power law, but since 2004 they are growing faster. If these two networks connect, they will form the largest network in Asia.

distribution. Comparison of the distributions of population relative to this gradient across deltas illustrates one of the principal morphologic differences among deltas.

The sub-kilometer resolution of the VIIRS DNB night light allows the current distribution of lighted development to be compared with delta morphology at comparable spatial scales. The much greater dynamic range of the VIIRS instrument clearly resolves brightness variations within urban areas to distinguish more brightly lighted transportation corridors and high density commercial and industrial areas whereas the OLS sensors were generally saturated in these areas. However, the combination of tri-temporal OLS night light and higher spatial resolution VIIRS night light shows the extent and evolution of lighted development that has occurred on the Asian megadeltas over the past 25 years, while preserving the more detailed brightness variations associated with the current urban structure. In addition to intra-urban structure, the much lower detection threshold of the VIIRS sensor resolves much smaller settlements and even vehicle lights on more heavily trafficked roads.

5. Conclusions

The analysis of Asian megadeltas described here combines recently released gridded population density (circa 2010) with a newly developed night light change product (1992 to 2012) and a digital elevation model to quantify the spatial distribution of population and development on the nine Asian megadeltas. Bivariate distributions of population as functions of elevation and coastal proximity quantify potential exposure of deltaic populations to flood and coastal hazards. While these data do not provide sufficient spatial or temporal resolution to serve as the basis for rigorous hazard assessments, they do provide a self-consistent basis for mapping the spatiotemporal evolution of development across deltas with very different fluvial and tectonic settings. As the required resolution can generally not be acquired retroactively, especially for deltas in developing countries, the observations given here provide a potentially valuable perspective on the evolution of urban development and potential exposure of population to flood-related hazards on nine of the most densely populated deltas in the world.

Comparison of these distributions for the Asian megadeltas show very different patterns of habitation with peak population elevations ranging from 2 to 11 m above sea level over a wide range of coastal proximities. Over all nine megadeltas, over 174 million people reside below a peak population elevation of 7 m. On three of the nine deltas (Changjiang, Pearl, Chao Phraya) dense urban populations are concentrated in close proximity to the coastline, potentially vulnerable to both fluvial and coastal hazards. The Changjiang and Pearl contain two of the most rapidly growing urban networks in Asia.

Changes in the spatial extent of anthropogenic night light from 1992 to 2012 show widely varying extents and changes of lighted urban development. All of the deltas except the Indus show the greatest increases in night light brightness occurring at elevations < 10 m. While this is probably beyond the elevation range of most storm surges, the fact that the cities are located within fluvial networks raises the possibility of multi-hazard impacts from combined river and coastal flooding.

At global and continent scales, growth of settlements of all sizes takes the form of evolving spatial networks of development. Spatial networks of lighted urban development in Asia show power law scaling properties consistent with other continents, but much higher rates of growth. While much of the urban growth observed in Asia occurs on inland agricultural plains, the three largest networks of development in China all occur on deltas and adjacent lowlands, and are growing faster than the rest of the urban network in China. Since 2000, the Huanghe Delta + North China Plain urban network has surpassed the Japanese urban network in size and may soon connect with the Changjiang Delta + Yangtze River urban network to form the largest conurbation in Asia.

Acknowledgements

CS gratefully acknowledges the support of NASA (grant NNX12AM20G) and the Office of Naval Research (grant N00014-11-1-0683). Work done by D. Sousa was conducted with Government support under FA9550-11-C-0028 and awarded by the Department of Defense, Air Force Office of Scientific Research, National Defense Science and Engineering Graduate (NDSEG) Fellowship, 32 CFR 168a. D. Sousa thanks E. Sousa for blazing the trail. The authors thank the editor and two anonymous reviewers for helpful comments and suggestions.

References

d'Amoura, C.B., et al., 2017. Future urban land expansion and implications for global croplands. Proc. Natl. Acad. Sci. 114 (34), 8939–8944.

Balk, D., et al., 2009. Understanding the impacts of climate change: linking satellite and other spatial data with population data. In: Guzman, J.M., Martine, G., McGranahan, G., Schensul, D., Tacoli, C. (Eds.), Population Dynamics and Climate Change. IIED/UNFPA, pp. 206–214.

Carabajal, C.C., Harding, D.J., 2006. SRTM C-band and ICESat laser altimetry elevation comparisons as a function of tree cover and relief. Photogramm. Eng. Remote Sens. 72 (3), 287–298.
Clauset, A., et al., 2009. Power-law distributions in empirical data. SIAM Rev. 51 (4), 661–703.
Elvidge, C.D., et al., 2013. What is so great about nighttime VIIRS data for the detection and characterization of combustion sources? Asia Pac. Adv. Netw. 33–48 (Honolulu, Hawaii).
Elvidge, C.D., et al., 2017. VIIRS night-time lights. Int. J. Remote Sens. 38 (21), 5860–5879.
Ericson, J.P., et al., 2006. Effective sea-level rise and deltas: causes of change and humandimension implications. Glob. Planet. Chang. 50, 63–82.
Gesch, D., et al., 2012. Validation of the Aster Global Digital Elevation Model Version 2 over the Conterminous United States. 2012 XXII ISPRS Congress. ISPR, Melbourne, Australia.
Gorokhovich, Y., Voustianiouk, A., 2006. Accuracy assessment of the processed SRTM-based elevation data by CGIAR using field data from USA and Thailand and its relation to the terrain characteristics. Remote Sens. Environ. 104, 409–415.
Hofton, M., et al., 2006. Validation of SRTM elevations over vegetated and non-vegetated terrain using medium footprint Lidar. Photogramm. Eng. Remote Sens. 72 (3), 279–285.
Hvidegaard, S.M., et al., 2012. ASTER GDEM validation using LiDAR data over coastal regions of Greenland. Remote Sens. Lett. 3, 85–91.
Imhoff, M.L., et al., 2004. The consequences of urban land transformation on net primary productivity in the United States. Remote Sens. Environ. 89, 434–443.
Jiang, C., et al., 2015. Impacts of urbanization on net primary productivity in the Pearl River Delta, China. Int. J. Plant Prod. 9 (4), 581–598.
Li, W., 2002. Zipf's law everywhere. Glottometrics 5, 14–21.
McGranahan, G., et al., 2008. A summary of the risks of climate change and urban settlement in low elevation coastal areas. In: Martine, G.M.G., Montgomery, M., Fernandez-Castilla, R. (Eds.), The New Global Frontier: Cities, Poverty and Environment in the 21st Century. Earthscan, pp. 165–182.
Meyer, D.J., et al., 2012. Summary of the Validation of the Second Version of the Aster GDEM. 2012 XXII ISPRS Congress. ISPRS, Melbourne, Australia.
Newman, M., 2010. Networks: An Introduction. Oxford University Press, Oxford, England.
Nicholls, R.J., et al., Canziani, O.F., Palutikof, J.P., van der Linden, P.J., 2007. Coastal systems and low-lying areas. In: Parry, M.L., Hanson, C.E. (Eds.), Climate Change 2007: Impacts, Adaptation and Vulnerability. Contribution of Working Group II to the Fourth Assessment Report of the Intergovernmental Panel on Climate Change. Cambridge University Press, Cambridge, UK.
Small, C., Cohen, J.E., 2004. Continental physiography, climate, and the global distribution of human population. Curr. Anthropol. 45 (2), 269–277.
Small, C., Nicholls, R.J., 2003. A global analysis of human settlement in coastal zones. J. Coast. Res. 19 (3), 584–599.
Small, C., Sohn, R., 2015. Correlation scales of digital elevation models in developed coastal environments. Remote Sens. Environ. 159, 80–85.
Small, C. and D. Sousa (2015). "Spatial scaling of land cover networks." ArXiv, https://arxiv.org/abs/1512.01517.
Small, C., Sousa, D., 2016. Humans on Earth; Global extents of anthropogenic land cover from remote sensing. Anthropocene 14, 1–33.
Small, C., et al., 2011. Spatial scaling of stable night lights. Remote Sens. Environ. 115, 269–280.
Smith, B., Sandwell, D., 2003. Accuracy and resolution of shuttle radar topography mission data. Geophys. Res. Lett. 30 (9) (20-21-24).
Sousa, D., Small, C., 2016. Spatial structure and scaling of agricultural networks. Remote Sens. Environ. 184, 615–627.
Syvitski, J.P.M., Saito, Y., 2007. Morphodynamics of deltas under the influence of humans. Glob. Planet. Chang. 57, 261–282.
Syvitski, J.P.M., et al., 2005. Impact of humans on the flux of terrestrial sediment to the global coastal ocean. Science 308, 376–380.
Syvitski, J.P.M., et al., 2009. Sinking deltas due to human activities. Nat. Geosci. 2, 681–686.
Tachikawa, T., et al., 2011. Characteristics of ASTER GDEM version 2. International Geoscience and Remote Sensing Symposium (IGARSS), IEEE.
Tadono, T., et al., 2012. Validation study on alos prism DSM mosaic and aster GDEM 2. 2012 XXII ISPRS Congress. ISPRS, Melbourne, Australia.
United Nations, D. o. E. a. S. A, Population Division, 2015. World Urbanization Prospects: The 2014 Revision, Highlights (ST/ESA/SER.A/352). United Nations, New York, USA.
Vörösmarty, C.V., Sahagian, D., 2000. Anthropogenic disturbance of the terrestrial water cycle. Bioscience 50, 753–765.
Woodroffe, C.D., et al., 2006. Landscape variability and the response of Asian megadeltas to environmental change. In: Harvey, N. (Ed.), Global Change and Integrated Coastal Mangement: The Asia Pacific Region. 10. Springer, Dordrecht, Netherlands, pp. 277–314.